MUNICH v2.0: A street-network model coupled with SSH-aerosol (v1.2) for multi-pollutant modelling

Youngseob Kim[1], Lya Lugon[1], Alice Maison[1,2], Thibaud Sarica[1], Yelva Roustan[1], Myrto Valari[3], Yang Zhang[4], Michel André[5], and Karine Sartelet[1]

[1]CEREA, École des Ponts, EDF R&D, Marne-la-Vallée, France
[2]Université Paris-Saclay, INRAE, AgroParisTech, UMR EcoSys, Thiverval-Grignon, France
[3]Laboratoire de Météorologie Dynamique, Sorbonne Université, École Polytechnique, IPSL, École Normale Supérieure, CNRS, Paris, France
[4]Department of Civil and Environmental Engineering, Northeastern University, Boston, MA, USA
[5]Department COSYS, Université Gustave Eiffel, Bron, France

Correspondence: Youngseob Kim (youngseob.kim@enpc.fr), Karine Sartelet (karine.sartelet@enpc.fr)

Abstract. A new version of the street-network model, Model of Urban Network of Intersecting Canyons and Highways version 2.0 (MUNICH v2.0) is presented. The comprehensive aerosol model SSH-aerosol is implemented in MUNICH v2.0 to simulate the street concentrations of multi pollutants including secondary aerosols. The implementation uses the Application Programming Interface (API) technology so that the SSH-aerosol version may be easily updated. New parameterisations are also introduced in MUNICH v2.0, including a non-stationary approach to model reactive pollutants, particle deposition and resuspension, and a parameterisation of the wind at roof level. A test case over a Paris suburb is presented for model evaluation and illustration of the impact of the new functionalities. The implementation of SSH-aerosol leads to an increase of 11% of PM_{10} concentration, because of secondary aerosol formation. Using the non-stationary approach rather than the stationary one leads to a decrease in NO_2 concentration by 16%. The impact of particle deposition on build surfaces and road resuspension on pollutant concentrations in the street canyons is low.

1 Introduction

More than half of the population now lives in urban areas (Ritchie and Roser, 2018), and is often exposed to high concentrations of nitrogen dioxide (NO_2) and fine particulate matter (PM) of diameters lower than and equal to $2.5\,\mu m$ ($PM_{2.5}$, Krzyzanowski et al., 2014). In many cities, there are densely built districts with street-canyon configurations. Street-level air quality has been reported to be worse than that in the surrounding area because of the presence of air pollutant sources. In particular, high concentrations of NO_2 (Cyrys et al., 2012), black carbon (Putaud et al., 2010; Lugon et al., 2021b), and organics have been reported (Putaud et al., 2010; Airparif, 2011).

Air quality models provide a useful tool to understand the phenomena of pollution in street canyons (Lugon et al., 2021b) and to estimate the impact of emission scenarios to reduce pollution. Different types of models may be used to represent the pollution in street canyons. Computational fluid dynamics (CFD) models describe finely the urban geometry, the air flow and the pollutant concentrations, e.g., Code_Saturne (Milliez and Carissimo, 2007; Thouron et al., 2019), OpenFOAM (Jeanjean

et al., 2015; Wu et al., 2021), STAR-CCM+ (Santiago et al., 2017), the PALM model (Wolf et al., 2020; Zhang et al., 2021). However, the computational cost is too high for operational purpose to predict the pollutant concentrations if applied to a city district with a large street network (at least hundreds street segments) (Vardoulakis et al., 2003). Parametric models are another type. They are suitable for operational purpose because of low computational cost. Some parametric models are based on a Gaussian dispersion methodology to represent emitted traffic-related pollutants, such as a Gaussian plume or puff, e.g., Polyphemus (Briant et al., 2013), CALINE4 (Benson, 1992), etc. Because they can not represent a street-canyon configuration, they are modified to include a specific module to represent this particular geometry, e.g. OSPM (Berkowicz, 2000), SBLINE (Namdeo and Colls, 1996), ADMS-Urban (McHugh et al., 1997). Other parametric models use parameterisations based on CFD modelling or wind-tunnel experiments to describe the flow in each street and the exchange from street to street, and between streets and the overlying atmosphere. The transport of pollutants from one street to another is taken into account through intersections, e.g. SIRANE (Soulhac et al., 2011) and the Model of Urban Network of Intersecting Canyons and Highways MUNICH (Kim et al., 2018). The flow above the street network is represented by a Gaussian dispersion methodology (SIRANE), or by one or two-way nesting to a regional model (MUNICH).

The streets are discretized with an Eulerian approach and boxes representing the street-segment volumes. Breaking away from the Gaussian methodology, this approach allows one to model the reactivity of pollutants as they are transported from the regional scale (background concentrations) to the street. Lugon et al. (2020) showed that it is crucial to couple the transport of pollutants in the street and chemistry finely, using a non-stationary approach avoiding a steady-state assumption, in order to represent the concentrations of reactive pollutants, such as NO_2. By coupling MUNICH to the aerosol model SSH-aerosol (Sartelet et al., 2020), Lugon et al. (2021a) showed that the formation of secondary aerosols is important not only at the regional scale, but also at the street level. This paper presents the version 2.0 of MUNICH. The different model improvements of Lugon et al. (2020, 2021a) have been implemented, as well as the modelling of deposition and resuspension of Lugon et al. (2021b). The coupling to the model SSH-aerosol has also been improved and automated. New parameterisations of the flow in the street are also added. A reference test case is presented for model evaluation and to illustrate the behaviour and the capabilities of MUNICH.

The description of the model along with major updates from v1.0 to v2.0 is summarized in section 2. Section 3 presents the simulation domain and the set up of the reference test case, which is compared to observations of NO_2, nitric oxide (NO), $PM_{2.5}$ and particulate matter of diameters lower than $10\,\mu m$ (PM_{10}). In sections 4, 5 and 6, different sensitivity simulations are presented to understand how these updates influence the street concentrations. They are classified depending on whether they concern transport (section 4), chemistry (section 5) and deposition/resuspension (section 6). Finally, two other sensitivity simulations on important parameters for the modelling and applications of MUNICH are performed (influence of building aspect ratio and effects of removing car traffic from specific streets).

2

2 Description of the model and major updates

The version 1.0 of MUNICH is described in Kim et al. (2018). Only the main concepts are reviewed here. In MUNICH, a street network is divided into street segments and intersections. A street segment is bounded by intersections with other street segments. A street segment is represented by one cuboid-type box and concentrations are assumed to be homogeneous in the corresponding volume, which is estimated as the product of segment length, width and average building height. The fluxes of pollutants emitted in a street segment, from human activities to natural sources (e.g. trees) are diluted within this volume. Pollutant concentrations are only evaluated in each street segment and not at intersections, which are defined to represent the street-to-street advective transfer of pollutants and part of the exchanges with the overlying atmosphere (Soulhac et al., 2009). The exchanges between a street segment and the overlying atmosphere are also computed at the top of each street segment. If the formulation of Salizzoni et al. (2009) is used, they depend on the standard deviation of the vertical wind velocity at roof level, which depends on atmospheric stability, and on the concentration gradients between the street and above. As detailed in MUNICH v1.0 (Kim et al., 2018), this formulation may be modified to take into account the influence of the street ratio (H/W), as suggested by Schulte et al. (2015), and detailed in Appendix B.

Pollutants are also advected from street to street after averaging the vertical wind profile in the street. This profile depends on the wind velocity at the roof level, which depends itself on the meteorological data above the streets (e.g., wind speed and direction) and the street segment characteristics (e.g., street segment direction, street width, building height). As detailed in MUNICH v1.0, two formulations may be used to represent the wind profile within the streets: the exponential formulation (Lemonsu et al., 2004) or the analytical formulation from SIRANE (Soulhac et al., 2008). These formulations depend on the wind velocity at the roof level u_H (see Appendix B), for which a new formulation is proposed here (see section 2.2 based on the work of Macdonald et al. (1998)).

Emission may be both in the gas and particle phases. The chemical transformations of the pollutants are modelled by a chemical kinetic mechanism for the gas-phase and/or by an aerosol model representing the aerosol dynamics (nucleation, condensation/evaporation and coagulation) and mass transfer between the gas and particle phases.

The loss fluxes due to deposition are represented through parameterisations of dry deposition and wet scavenging. An approach to estimate resuspension is added in MUNICH v2.0, following Lugon et al. (2021b).

Many modelling options are included to represent the different physico-chemical processes taken into account in MUNICH. They are presented in Appendix B. A demonstration test case is set up in section 2.1 to illustrate how the pollutants are transported within the street network from a single emission source. This test case is used for model validation from one version of MUNICH to the next. Then, the section describes the new features in comparison to MUNICH v1.0.
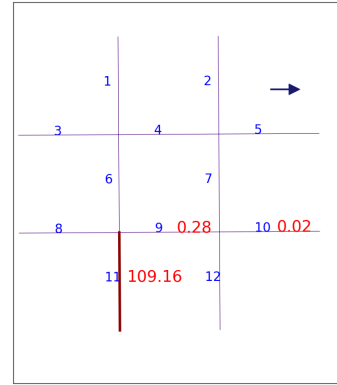
2.1 Advection through intersections

At intersections, the pollutant mass flux from one street to others can be computed by estimating the balance of the air-volume fluxes among the streets that are connected to the intersection.
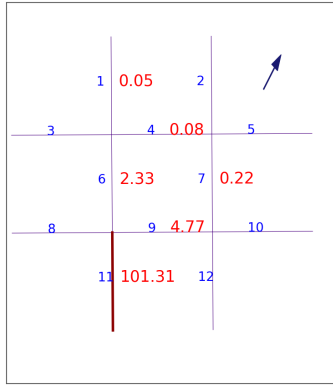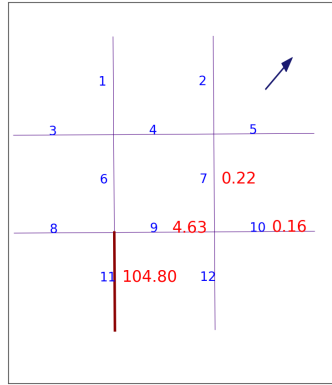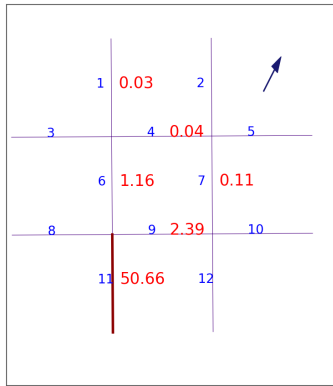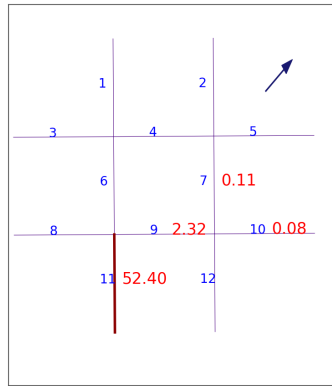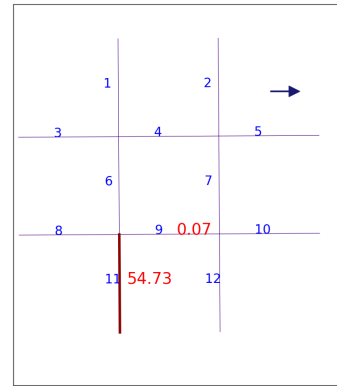
Figure 1. Variation of pollutant concentrations in a street network depending on wind direction, which are indicated as arrows in dark blue. The wind speed is $5\,\mathrm{m\,s^{-1}}$ for the upper three cases and $10\,\mathrm{m\,s^{-1}}$ for the lower three cases. The wind direction is given from the North (top of the figure). The blue numbers are the street ID and the red numbers are the concentrations in $\mathrm{\mu g\,m^{-3}}$. Pollutant is emitted only in the street segment 11.

85   A simplified street network with 12 street segments was designed to perform a theoretical test case and illustrate how mass fluxes are modelled. For simplicity, the wind speed at roof top is fixed to an arbitrary value (5 or 10 m s^{-1}), and a pollutant is emitted in only one single street segment (number 11 in Figure 1). Figure 1 displays the mass concentration calculated using MUNICH in the different street segments (red numbers). The concentrations are the highest in the street segment where the pollutant is emitted. The concentrations vary depending on the wind direction above the streets. For higher wind speed at the

90   roof level (10 m s^{-1}, see Figures 1d-f), the pollutant concentrations are lower over all street segments. This is due to an increase in the advection and also an increase in the vertical transfer by turbulence at rooftop.

4

2.2 Wind velocity at the roof level

The computation of the vertical wind profile within the street depends on the wind velocity determined at the roof level u_H (see equations B12 and B13 of Appendix B). u_H was computed following Soulhac et al. (2008) in MUNICH v1.0, based on a 2D parameterisation of the wind field along the street axis. Now it may be computed depending on the street characteristics using a logarithmic wind profile above the buildings, as defined in Macdonald et al. (1998). This wind profile corresponds to an average profile over a relatively large urban-scale area, such as a relatively homogeneous district or city. It is based on the calculation of a displacement height (d_c) and a roughness length (z_{0c}) for the homogeneous urban canopy area (district) considered. Note that the roughness length of the district is typically on the order of $1\,\mathrm{m}$ (see Figure 2) whereas those of street walls and road pavement are on the order of $1\,\mathrm{mm}$.

$$\frac{d_c}{\overline{H}} = 1 + \Delta^{-\lambda_P} \left(\lambda_P - 1\right) \tag{1}$$

$$\frac{z_{0c}}{\overline{H}} = \left(1 - \frac{d_c}{\overline{H}}\right) \exp\left(-\left(0.5\delta \frac{C_{D_b}}{\kappa^2}\left(1 - \frac{d_c}{\overline{H}}\right)\lambda_F\right)^{-0.5}\right) \tag{2}$$

where Δ and δ are empirical constants ($\delta = 1.0$ and $\Delta = 4.43$ for staggered arrays ; $\delta = 0.55$ and $\Delta = 3.59$ for square arrays; Macdonald et al. 1998, the values for staggered arrays are used in MUNICH v2.0), C_{D_b} is the building drag coefficient usually equal to 1.2 (Macdonald et al., 1998), κ is the von Kármán constant ($\kappa = 0.41$).

λ_P and λ_F are respectively the plan and frontal area densities of obstacles calculated as:

$$\lambda_P = \frac{A_P}{A_T} = \frac{\overline{W_{building}}\,\overline{L}}{\left(\overline{W_{building}} + \overline{W_{street}}\right)\overline{L}} \quad \text{and} \quad \lambda_F = \frac{A_F}{A_T} = \frac{\overline{H}\,\overline{L}}{\left(\overline{W_{building}} + \overline{W_{street}}\right)\overline{L}} \tag{3}$$

A_F, A_P and A_T are respectively the frontal, plan and lot area of obstacles (A_T corresponds to the total area divided by the number of obstacles). Those surface ratios are calculated from the average characteristics of the streets in the district considered: building height ($\overline{H}$), street width ($\overline{W_{street}}$), building width ($\overline{W_{building}}$) and street length ($\overline{L}$), which cancels in the both equations.

Finally, u_H is calculated for each street of building height H as:

$$u_H = \frac{u_*}{\kappa} \ln\left(\frac{H - d_c}{z_{0c}}\right) = u_{ref} \times \frac{\ln\left(\frac{H - d_c}{z_{0c}}\right)}{\ln\left(\frac{z_{ref} - d_c}{z_{0c}}\right)}. \tag{4}$$

Depending on the chosen input parameters, u_H can be calculated from the friction velocity u_* (in $\mathrm{m.s}^{-1}$) defined at urban canopy scale or from a wind speed at a reference altitude above the street ($u(z_{ref}) = u_{ref}$ in $\mathrm{m.s}^{-1}$). For each street, only the axial component of u_H is considered to compute the average wind speed in the street direction. Therefore, the horizontal transport of pollutants in the street depends on the angle between the wind direction and the street orientation.
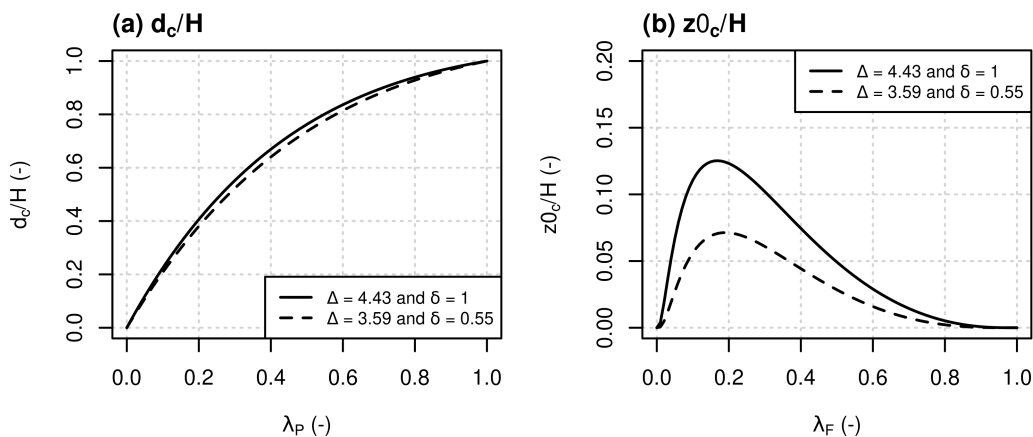
(a) d_c/H

(b) $z0_c/H$

Figure 2. $d_c/\overline{H}$ and $z_{0_c}/\overline{H}$ as a function of the plan and frontal area densities calculated with Macdonald et al. (1998) equations.

2.3 Concentrations of reactive species: non-stationary approach

In MUNICH v1.0, a first-order splitting scheme between "transport" (including removal processes) and chemistry is used to calculate the concentrations in a street segment, with fixed splitting time steps (typically 100 s). This numerical approach holds

125 for slowly-reacting species, but it fails to represent the temporal evolution of fast-reacting species. The characteristic time scales of fast chemical processes may be similar to (or faster than) those of transport in and out the street. A new algorithm is presented in Lugon et al. (2020) to remove the steady-state assumption for transport (i.e. the stationary approach). At the first time iteration, the characteristic time scale of transport is estimated, then transport and chemistry are solved sequentially on a time step corresponding to this characteristic time. Transport is solved using an explicit two-stage Runge-Kutta algorithm

130 (explicit trapezoidal rule of order 2) or a semi-implicit Rosenbrock algorithm, and chemistry is solved with smaller time steps using a Rosenbrock algorithm or the solver used in SSH-aerosol (two-stage Runge-Kutta or two-step algorithms). The equations for gas-phase chemistry and aerosol dynamics (grouped here as "chemistry") are solved using sub-time steps, because they correspond to a stiff set of equations with very fast processes such as radical chemistry. The time step is adapted depending on the evolution of the concentrations due to transport-related processes.

135 Using a beta version of MUNICH, Lugon et al. (2020) showed that this algorithm is numerically stable for reactive species, unlike the one using the stationary assumption. The effects of this new algorithm in MUNICH v2.0 are presented in section 5.2.

2.4 Coupling to SSH-aerosol (v1.2)

The chemical composition of particles in streets differs from those above, mostly because of emitted pollutants within the street, for example from traffic (Lugon et al., 2021a). Within the streets, emitted pollutants mix with those from above the

140 street and undergo chemistry. In MUNICH v1.0, only gas-phase chemistry is taken into account, and the CB05 chemical kinetic mechanism (Yarwood et al., 2005) is implemented to simulate the gas-phase concentrations (Kim et al., 2018).
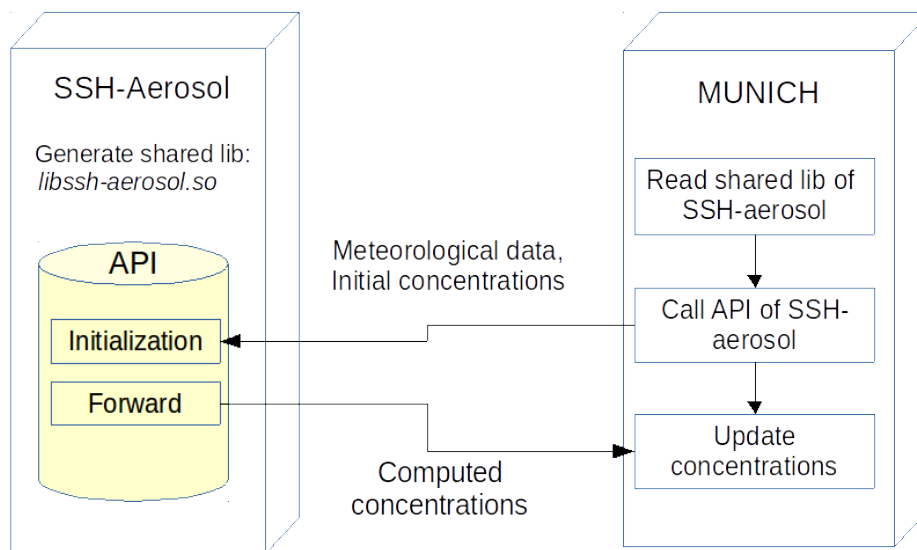
6

Figure 3. Schematic diagram of the coupling of SSH-aerosol with MUNICH using the API.

In MUNICH v2.0, the SSH-aerosol model (Sartelet et al., 2020) may be used to simulate both gas-phase chemistry and aerosol thermodynamics and dynamics (i.e., nucleation, condensation/evaporation, and coagulation). SSH-aerosol is designed to be easily implemented into other models. It contains an Application Programming Interface (API), designed to allow for easy version updates. The API is used to implement SSH-aerosol v1.2 into MUNICH v2.0. The schematic diagram of coupling using the API is illustrated in Figure 3. A previous version of SSH-aerosol was implemented in MUNICH without using the API (Lugon et al., 2021a); it reproduced satisfactorily measured PM_{10} and $PM_{2.5}$ concentrations in the streets of Paris, taking into account the formation of secondary inorganic and organic aerosols. The influence of secondary aerosol formation is presented in section 5.1.

2.5 Resuspension and deposition

Lugon et al. (2021b) introduced a new approach in MUNICH to estimate particle resuspension in streets. This approach strictly ensures the mass balance on the street surface. To do that, the accurate modelling of particle deposition and wash-off by water is mandatory. In MUNICH v2.0, the particle deposition is computed considering the available surface area including pavement area and building walls as proposed in Cherin et al. (2015). For the particle wash-off, the amount of water on the street surface is computed from the meteorological conditions. Solubility of species is also an important factor for the wash-off parameterisation.

Modelling of the particle resuspension in MUNICH v2.0 requires an estimation of a resuspension factor. The resuspension factor is computed considering the traffic flow characteristics such as vehicle flow and speed, as detailed in Lugon et al. (2021b). The sensitivity of concentrations to deposition and resuspension is presented in section 6.

7

3   Reference test case

MUNICH v2.0 is applied to simulate the pollutant concentrations over a Paris suburb. The reference test case is set up over a district in the eastern part of Greater Paris between 22 March and 13 May 2014, which corresponds to a period when street measurements were performed, with samples taken at a height of about 3 m (TRAFIPOLLU project, see the location of the station in Figure 4a). The street network of the domain consists of 577 street segments and is displayed in Figure 4a. The input
165   data used for this study are now detailed. They are summarized in Table 1. The simulated concentrations are then compared to street observations.

3.1   Input data

3.1.1   Traffic emissions

Traffic-related emissions in streets are computed using Pollemission (Sarica, 2021), which relies on emission factors from the
170   COPERT methodology (COmputer Program to calculate Emissions from Road Transport, version 2019, EMEP/EEA, 2019) and the vehicle fleet. Emission factors are provided by the COPERT methodology for a wide range of vehicles types, depending on fuel type and European emission standard. The COPERT methodology is used for emission factors from both exhaust and non-exhaust, i.e., wears of tyres and brakes and vehicle-induced abrasion of the road. Simulations using the dynamic
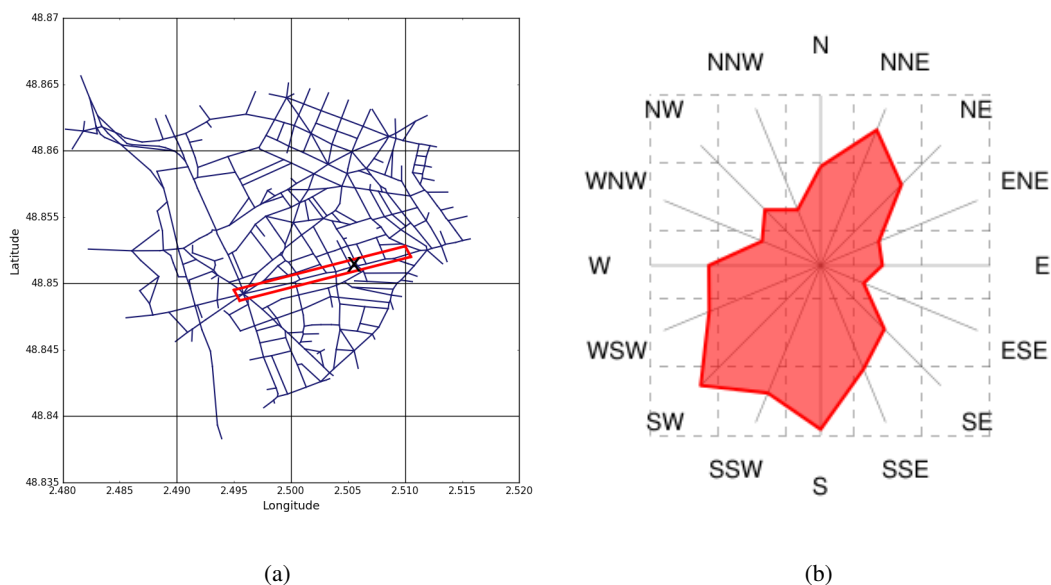

(a)   (b)

Figure 4. (a) Street network of the domain. The street named "Boulevard Alsace Lorraine", where measurements were performed, is highlighted in the red box. The black cross mark corresponds to the location of the air monitoring station. (b) Occurrence number of wind direction over the street network for the period from 22 March to 13 May 2014.

Table 1. Input data for MUNICH simulation.

Data	Source	Reference
Traffic emissions	Dynamic traffic model Symuvia and Pollemission for emission data	Leclercq et al. (2007), https://doi.org/10.5281/zenodo.5721253
Geographic data	BD TOPO database ("Base de Données TOPOgraphiques")	https://geoservices.ign.fr/bdtopo (in French) as used in Kim et al. (2018)
Meteorological data	WRF simulation (v3.9.1.1)	Lugon et al. (2020)
Background concentrations	Polair3d simulation	Sartelet et al. (2018); André et al. (2020)

traffic model SymuVia (Leclercq et al., 2007) provided, for each street segment of the network, the number of vehicles and
175 speed profiles per hour and per category (passenger cars, light commercial vehicles, heavy-duty vehicles...) for a weekday
and a weekend day. The vehicle fleet is mainly composed of passenger cars and light commercial vehicles, 77 % and 14 %
respectively on average. In each category, the breakdown by fuel and European standard is based on André et al. (2019). For
each vehicle type, hourly profiles of vehicle flows and averaged speeds for a weekday and a weekend day are then used with
COPERT emission factors to estimate the traffic emissions over the whole period (22 March to 13 May 2014).

180 Nitrogen oxides (NO_x) emission factors are speciated into NO and NO_2 using the fractions of NO_2 provided by the COPERT
methodology for each vehicle type. Speciation of PM emission factors also follows the COPERT methodology by using the
fractions of black carbon (BC) and organic matter (OM) supplied for each vehicle type. The OM fraction of the PM emissions
is assumed to be emitted as low-volatility organic compounds (LVOC) in the particle phase. If a fraction of PM remains after
the BC and OM speciation, it is categorised as dust and unspeciated species. The PM size distribution at emission is assumed
185 to be the same as in Lugon et al. (2021a, b), i.e. exhaust primary PM is assumed to be in the size bin [0.04 – 0.16 μm] while
non-exhaust primary PM is coarser, i.e., in the size bin [0.4 – 10 μm].

Non-methane volatile organic compounds (NMVOC) emission factors are computed as the difference between volatile
organic compounds (VOC) and methane emission factors. In contrast to NO_x and PM, the COPERT methodology presents
five NMVOC speciation profiles given the fuel and category of the vehicle. These profiles include approximately 60 different
190 species up to about C9 (9 carbon atoms) and lumped species for heavier compounds. Intermediate volatility organic compounds
(IVOC) thus include the alkanes C10-C12, cycloalkanes, aromatics C9 and aromatics C10. Similarly, semi-volatile organic
compounds (SVOC) include the alkanes C>13 and aromatics C>13. Both IVOC and SVOC are emitted in the gas phase in the
simulation, and the partitioning between the gas and particle phases is treated by the model when computing concentrations.

3.1.2 Geographic data

195 The widths of vehicle lane in the streets, street lengths and average building heights were obtained from the BD TOPO database
("Base de Données TOPOgraphiques", https://geoservices.ign.fr/bdtopo). The information for the sidewalk width and the high-
way shoulder width (the A86 highway passes through the modelling domain) is not available in the BD TOPO database. A

width of 3 m is used for sidewalk of the streets, and 20 m (including two urban train lanes) for the shoulder of the A86 highway (Kim et al., 2018).

3.1.3 Regional-scale data

Meteorological data at a 1 km x 1 km horizontal resolution were obtained from Lugon et al. (2020), who conducted a simulation using the Weather Research and Forecasting (WRF) model version 3.9.1.1 (Skamarock et al., 2008). In the WRF model setup, the single-layer urban canopy model (UCM) was used to represent the urban meteorological condition (Kusaka et al., 2001). The meteorological data from the WRF simulation are updated every hour in the MUNICH simulations, and they are interpolated for the times between each hour. Figure 4b shows the occurrence of wind direction over the simulation domain for the period from 22 March to 13 May 2014. The occurrence of wind direction is counted for wind that comes from each compass direction (N, NNE, NE, etc). South and Southwest winds are the prevailing winds during the simulation period.

Background concentrations above the streets are obtained from the simulation results of the 3-dimensional chemical-transport model Polair3D (Sartelet et al., 2007). The Polair3D simulation is presented in Sartelet et al. (2018); André et al. (2020). The same chemical scheme is used in the MUNICH simulation as in the Polair3D regional-scale simulation (CB05 with additional semi-volatile organic aerosols as detailed in Kim et al., 2011, Chrit et al., 2017 and Sartelet et al., 2020).

3.2 Simulated concentrations

The reference test case (Case-1) is performed for the period from 22 March to 13 May 2014 using the options of Table 2. In Figure 5, computed 24 h averaged concentrations are compared to the observed concentrations at the air monitoring station operated by Airparif during the TRAFIPOLLU project.

Two distinct statistical criteria are used to evaluate the model performance for hourly concentrations: an acceptance and a strict criteria (Hanna and Chang, 2012; Herring and Huq, 2018), see Table 3. The corresponding statistical indicators are defined in Appendix A1.

The hourly NO_2 concentrations estimate well the observations: the acceptance criteria are validated for all statistical indicators, and the strict criteria are validated for almost all indicators: the fractional bias (FB) is equal to -31%, while it should be lower than 30% to satisfy the strict criteria. However, the NO concentrations are strongly underestimated, and do not satisfy the acceptance criteria. These discrepancies were observed in the previous studies (Kim et al., 2018; Lugon et al., 2020). The discrepancies in the simulation results using MUNICH v2.0 are reduced compared to those using MUNICH v1.0 but they are still high. The discrepancies can be explained by uncertainties in the traffic emission data, the vertical transfer at rooftop and the lifetime of NO (Kim et al., 2018; Lugon et al., 2020).

The statistical indicators for the simulated PM_{10} and $PM_{2.5}$ concentrations are also satisfactory. For PM_{10} concentrations both the acceptance and strict criteria are met for the different indicators. For $PM_{2.5}$ concentrations the acceptance criteria are met for the different indicators, but they do not meet the strict criteria for the FB, the normalized mean square error (NMSE) and the mean geometric bias (MG). The FB is equal to 34%, while it should be lower than 30% to satisfy the strict criteria. The overprediction for the $PM_{2.5}$ concentrations may be due to the uncertainties in the size distribution and non-exhaust emissions.

10

(Lugon et al., 2021a) showed that the observed and simulated $PM_{2.5}/PM_{10}$ ratios are lower at traffic stations (47% to 66%) than at urban background stations (67% to 76%) because of high non-exhaust emissions, mostly emitted as coarse particles. In the reference simulation, the observed $PM_{2.5}/PM_{10}$ ratio is 51%. However the simulated ratio is 89%.

Figure 6a shows the time-averaged concentrations over the simulation domain for the simulated $PM_{2.5}$ concentrations. The concentrations are high over the major streets where the emission rates are high.

Table 2. List of used options in the reference simulation.

Option type	Used option
Solver	Explicit Trapezoidal Rule of order 2 (ETR)
Stationary approach	No
Turbulent vertical flux at the roof level	SCHULTE
Mean wind speed in the street canyon	Exponential
Wind speed at the roof level	SIRANE
Wind profile for deposition	MASSON
Resuspension	No
Chemistry (gas-phase chemistry and aerosol formation pathways)	Yes
Deposition	Yes

Table 3. Statistical indicators of the comparison of simulated hourly concentrations to the measurements at the air monitoring station.
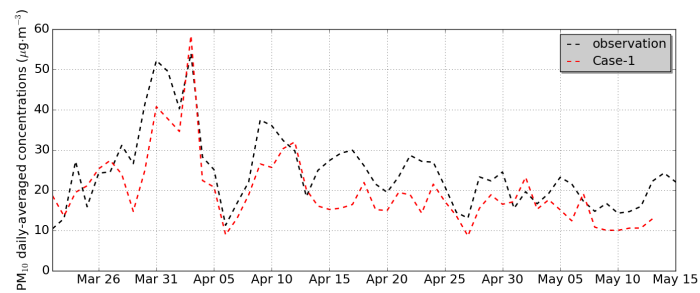
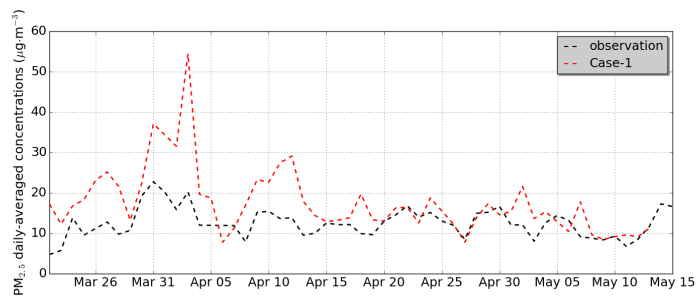|	NO$_2$	NO	PM$_{10}$	PM$_{2.5}$	Strict criteria	Acceptance criteria
Observation ($\mu g\,m^{-3}$)	54.4	68.1	24.6	12.5		
Simulation ($\mu g\,m^{-3}$)	39.8	22.9	19.7	17.6		
FB	-0.31	-0.99	-0.22	0.34	-0.3 < FB < 0.3	-0.67 < FB < 0.67
NMSE	0.28	1.54	0.21	0.44	NMSE < 0.3	NMSE < 0.6
MFE	0.46	1.00	0.38	0.47		
VG	1.42	6.18	1.27	1.52	VG < 1.6	
MG	0.68	0.30	0.80	1.38	0.7 < MG < 1.3	
FAC2	0.75	0.20	0.84	0.74	FAC2 $\geq$ 0.5	FAC2 $\geq$ 0.3
NAD	0.22	0.49	0.19	0.25	NAD < 0.3	NAD < 0.5
R	0.58	0.76	0.68	0.48		
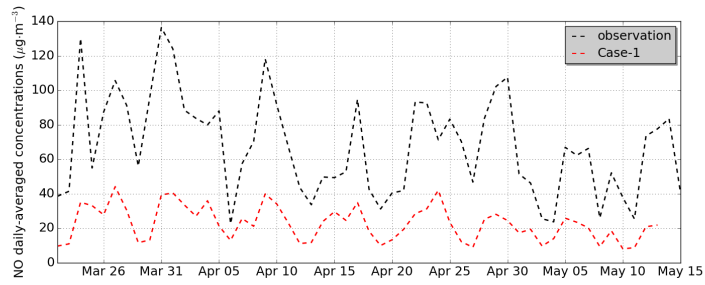
(a) NO
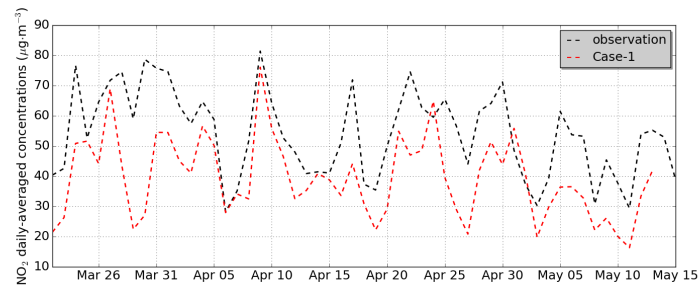
(b) NO$_2$

(c) PM$_{10}$

(d) PM$_{2.5}$

Figure 5. Comparison of daily concentrations (in $\mu g\,m^{-3}$) in Case-1 (reference) simulation to the measurements at the monitoring station for (a) NO and (b) NO$_2$ (c) PM$_{10}$, (d) PM$_{2.5}$.

Several simulations (sensitivity test cases) were performed to estimate the influence of the different model options on the computed concentrations. In each sensitivity test case, one parameterisation or process is modified with respect to the reference simulation. The characteristics of the simulations are listed in Table 4 and the available model options are explained in Appendix B. These sensitivity test cases are presented in the following sections. Domain-averaged normalized mean error (NME)

240 between the sensitivity test case and the reference simulation is computed: a NME is computed for each street over the whole simulation period and then averaged over the simulation domain. Larger domain-averaged NME means larger influence of the model option tested in the sensitivity test case.

Table 4. List of test cases and normalized mean error (NME, see Appendix A) between the sensitivity test case and the reference simulation (Case-1). The NME is computed for $PM_{2.5}$ and NO_2 for each street over the whole simulation period and then averaged over the whole simulation domain.

Name of the test case	Changed option	NME for $PM_{2.5}$	NME for NO_2
Case-1 (Reference)	-	-	-
Case-2	Without chemistry	13%	11%
Case-3	Without deposition	1%	2%
Case-4	With resuspension	1%	0%
Case-5	Stationary approach	6%	16%
Case-6	Rosenbrock solver	0%	0%
Case-7	Turbulent vertical transfer at the roof level: SIRANE	1%	4%
Case-8	Mean wind speed in the street canyon: SIRANE	1%	1%
Case-9	Turbulent mixing at intersection	1%	1%
Case-10	Wind speed at the roof level: MACDONALD	13%	32%

## 4   Influence of parameters related to transport

This section investigates the influence on concentrations of parameters related to transport, i.e. to the description of the wind
245 velocity and the turbulence. Amongst the different parameterisations tested (Case-7, Case-8, Case-9 and Case-10), the estimation of the wind velocity at the roof level (Case-10) is the most influential. It directly impacts the strength of the wind speed within streets.

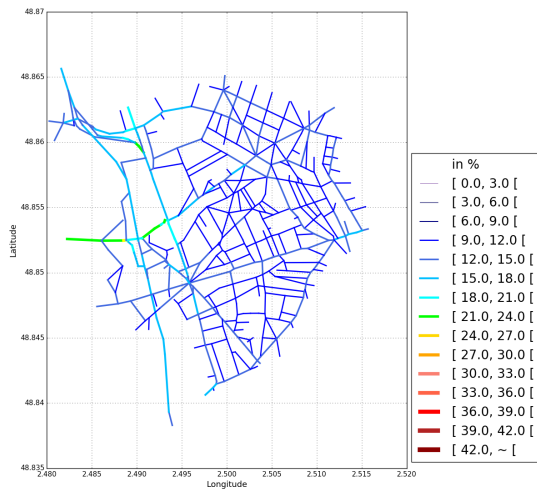### 4.1   Wind velocity at the roof level

Two parameterisations may be used to compute the wind velocity at the roof level (u_H). In MUNICH v1.0, u_H was computed
250 with SIRANE parameterisation following Soulhac et al. (2011). The MACDONALD parameterisation is added in MUNICH
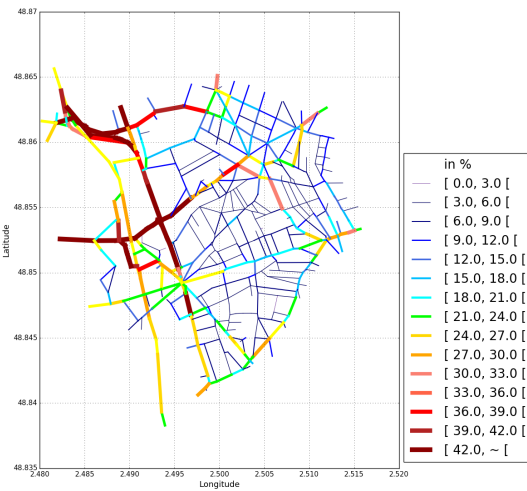
13
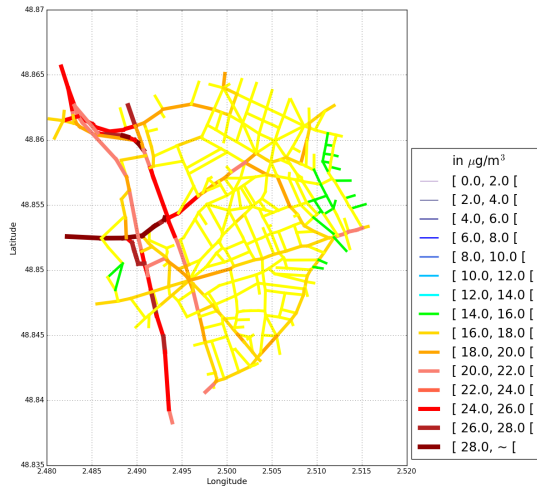
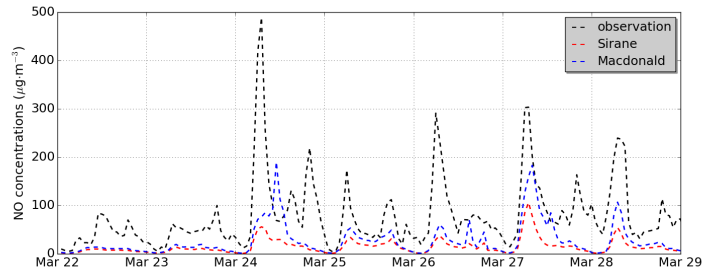(a) Case-1, PM$_{2.5}$ concentration
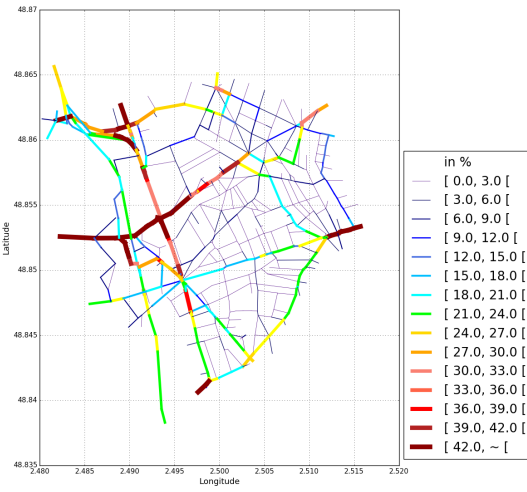
(b) NME between Case-10 and Case-1

(c) NME between Case-2 and Case-1

(d) NME between Case-11 and Case-1

Figure 6. PM$_{2.5}$ time-averaged concentrations (in µg m^{-3}) for the reference test case (Case-1, upper left panel) and normalised mean error (NME, %) between a sensitivity test case and the reference test case, which quantifies the average impact of parameterisations on the concentrations (Case-10 in the upper right panel, Case-2 in the lower left panel and Case-11 in the lower right panel). The absolute differences in the concentrations between the simulations are presented in additional figures in Appendix C.

(a) NO
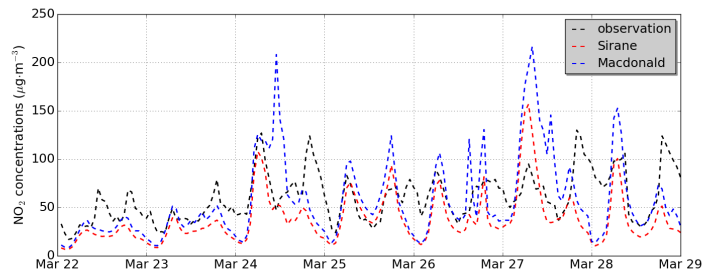
(b) NO$_2$

Figure 7. Comparison to observation of NO and NO$_2$ hourly concentrations (in $\mu g\,m^{-3}$) using two different parameterisations to compute the wind velocity at the roof level: SIRANE (Case-1) in red and MACDONALD (Case-10) in blue.

v2.0, as detailed in section 2.2. The MACDONALD parameterisation is used in Case-10 simulation. An increase in both NO (NME of 55%) and NO$_2$ (NME of 32%) concentrations is observed with the MACDONALD parameterisation, see Figure 7.

For the comparison with the observation data, the MACDONALD parameterisation better simulates NO concentration than the SIRANE parameterisation. However the MACDONALD parameterisation overestimates the peaks of NO$_2$ concentrations.

Figure 6b shows the time-average NME (NME computed on the basis of temporal series) over the different street segments of the simulation domain for the PM$_{2.5}$ concentrations. The NME are high where the concentrations are high. The MACDONALD parameterisation leads to an increase of concentrations at the air monitoring station with a NME of about 15% and the maximum NME over the street domain is about 50% (13% over the whole domain).

Because the MACDONAL parameterisation better estimated the roof-level wind speeds than the SIRANE one, in comparison to the CFD simulation results of Maison et al. (2022), the MACDONALD parameterisation is recommended in MUNICH. However, because of uncertainties on the regional wind speed and friction velocity, simulations with the SIRANE parameterisation could give better scores compared to observations for some applications.

4.2 Turbulent transfer at the roof level

Two parameterisations are available to compute the turbulent vertical flux in MUNICH: SIRANE and SCHULTE. In the first one, the vertical flux is computed taking into account the street length and the street width. In the second one, the building height is also considered.

The sensitivity of the concentrations to this option is estimated by comparing the Case-7 simulation to the Case-1 simulation. Figure 8 presents a comparison to observation of NO_2 and $PM_{2.5}$ hourly concentrations in the Case-1 and Case-7 simulations. The time-averaged NME, between Case-1 and Case-7, presented in Table 4, are low (1% for $PM_{2.5}$ and 4% for NO_2). However, the differences between Case-1 and Case-7 are important for the peak concentrations during morning and evening rush hour. The peak concentrations of NO_2 in the Case-7 simulation (in blue line) are larger than those in the Case-1 simulation (in red line), by up to 30%. The largest differences are on March 24 evening and March 28 morning. For $PM_{2.5}$, the peak concentrations are less sensitive to the parameterisation of turbulent transfer, and the maximum difference between the two cases is 13% on March 27 morning.

Kim et al. (2018) showed that the vertical flux is higher with SCHULTE than SIRANE in areas with low buildings. On the contrary, the vertical flux is lower with SCHULTE than SIRANE in areas with tall buildings. The concentrations are then higher with the SIRANE parameterisation on the simulation domain where the building heights are low.

Because the SCHULTE parameterisation for the turbulent vertical mass transfer at roof-level includes an additional dependence to the street aspect ratio compared to SIRANE one, leading to better comparisons to the CFD simulations of Maison et al. (2022), the SCHULTE parameterisation is recommended in MUNICH.

## 4.3 Wind speed formulation within the street and turbulent mixing at intersections

In the Case-8 simulation, the mean wind speed in the street canyon is calculated using the SIRANE parameterisation instead of the Exponential parameterisation in Case-1. Kim et al. (2018) showed that the impact of the mean speed using the SIRANE or Exponential parameterisation is low for streets of low aspect ratio (about 1/3). The time-averaged NME between the Case-1 and Case-8 over the street network is also low: about 1% for $PM_{2.5}$ and 1% for NO_2.

Soulhac et al. (2011) suggested that the turbulent mixing at intersections can be represented by considering horizontal fluctuations in the wind direction. These horizontal fluctuations are parameterised using a Gaussian distribution of the wind direction, as detailed in Appendix B. The influence of the parameterisation of the turbulent mixing at intersections is tested in the Case-9 simulation. The time-averaged NME between Case-1 and Case-9 are low: about 1% for $PM_{2.5}$ and 1% for NO_2.

Because the comparison to CFD simulations shows that the exponential profile overestimates the wind speed in the street especially at the bottom of the street (Maison et al., 2022), the SIRANE parameterisation is recommended for the horizontal wind speed within the street. Taking into account horizontal fluctuations in the wind direction is not necessary, because of its low influence on concentrations.
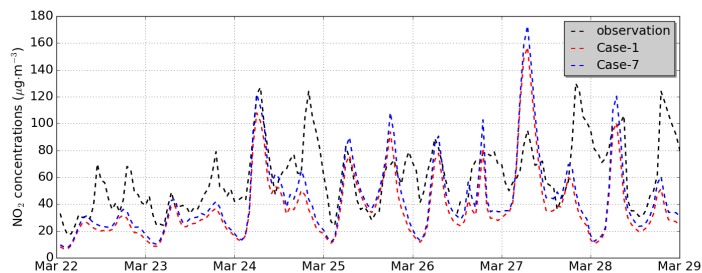
(a) NO$_2$
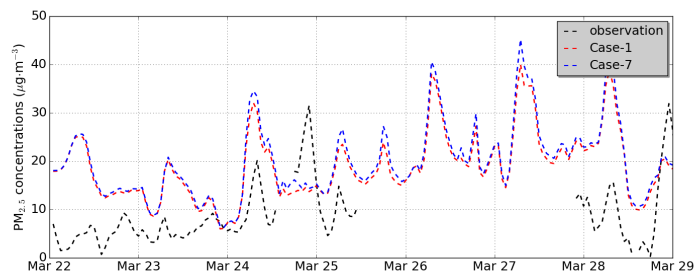
(b) PM$_{2.5}$

Figure 8. Comparison to observation of NO$_2$ and PM$_{2.5}$ hourly concentrations (in $\mu g\,m^{-3}$) using SCHULTE (Case-1) in red line and SIRANE (Case-7) in blue line.

5 Influences of parameters related to secondary pollutant formation

5.1 Secondary gaseous and aerosol species

In the simulation Case-2, the aerosol model SSH-aerosol is not used, and the pollutant concentrations are computed taking into account only emission, deposition and transport processes. Figure 6c shows the time-averaged NME over the simulation domain for the PM$_{2.5}$ concentrations between the Case-1 and Case-2 simulations. The NME over the whole domain for the PM$_{2.5}$ concentrations is 13%. Note that high NME are obtained over some major streets. Figure 9 presents the NME between the Case-1 and Case-2 simulations for the total PM$_{10}$ concentration and the concentrations of inorganic/organic aerosols. The concentrations of PM$_{10}$ are reduced (NME of 11%) when chemistry and aerosol dynamics are not modelled. The reduction is due to the absence of secondary inorganic and organic aerosol formation in the simulation Case-2. For inorganic aerosols, the concentrations of ammonium and nitrate in Case-2 are lower (NME of 24% and 5%, respectively). Very low change in sulfate is obtained. For organic aerosols, the concentrations of particles that are formed from natural sources are lower (NME of 74%) than those formed from human activities (NME of 13%). The NME for total organic aerosol is 43%.

For the gas-phase species, the absence of conversion from NO to NO$_2$ by the chemical reactions in Case-2 leads to a reduction of NO$_2$ in Case-2 (NME of 11%).
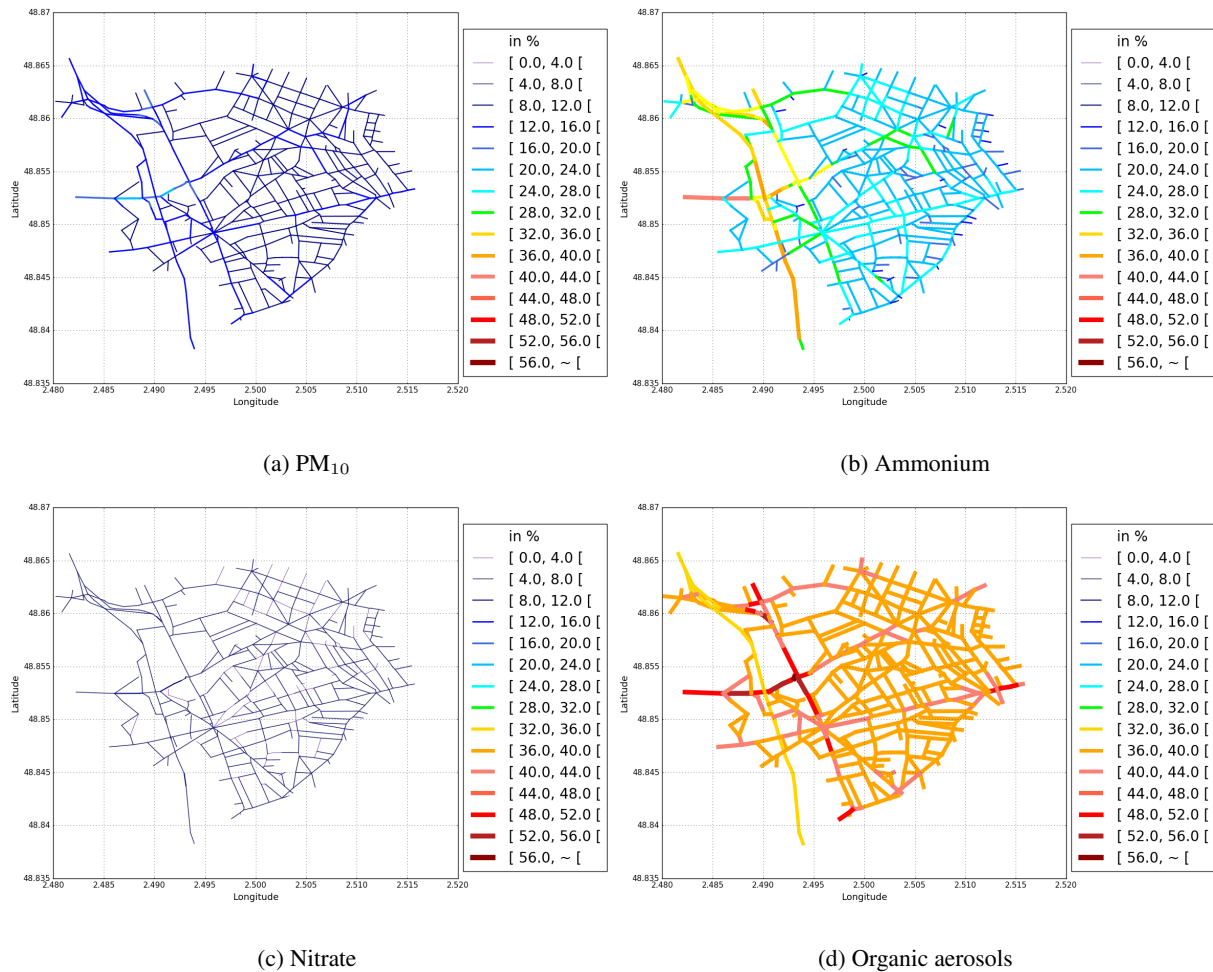
17

(a) PM$_{10}$

(b) Ammonium

(c) Nitrate

(d) Organic aerosols

Figure 9. Temporal NME (in %) between Case-1 and Case-2 for (a) PM$_{10}$, (b) Ammonium, (c) Nitrate and (d) Organic aerosols. The absolute differences in the concentrations between the simulations are presented in additional figures in Appendix C.

As a large fraction of NO$_2$ is secondary, formed from the conversion of primary NO by ozone titration (Lugon et al., 2020), it is crucial to take gas-phase chemistry into account to accurately represent NO$_2$ concentrations. The inorganic and organic concentrations of PM are strongly influenced by aerosol dynamics, mostly because of the condensation/evaporation process (e.g. NH$_3$ from traffic emission condenses with existing HNO$_3$). However, the coagulation process also needs to be taken into account to accurately represent the particle size distribution (Lugon et al., 2021a).

5.2 The non-stationary approach

In the simulation Case-5, the stationary hypothesis is assumed to compute the pollutant concentrations. As shown in Lugon et al. (2020) and Figure 10, higher concentrations of NO$_2$ are obtained in the simulation Case-5 than in Case-1 with a temporal
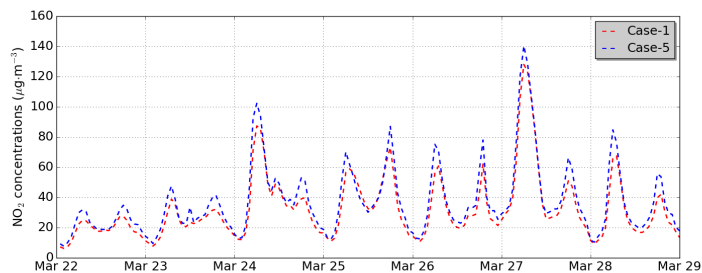
(a) NO$_2$
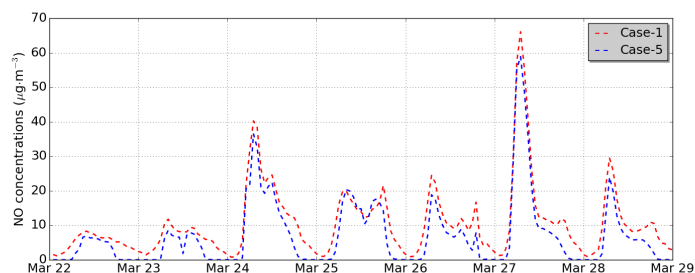
(b) NO

Figure 10. Comparison of (a) NO$_2$ and (b) NO hourly concentrations using the non-stationary approach (Case-1) in red and the stationary approach (Case-5) in blue. The concentrations are averaged over the whole simulation domain.

NME of 35% for the Boulevard Alsace Lorraine and 16% on average over the domain). This increase in NO$_2$ concentration using the stationary hypothesis may be due to more conversion from NO to NO$_2$; the NO$_x$ concentration are similar between Case-1 and Case-5, the time-averaged NME are lower than 1%. Figure 11 presents the time-average NME in the concentrations simulated between Case-5 and Case-1. For PM$_{10}$ and PM$_{2.5}$, time-averaged NME are not as high as for NO$_2$. The NME is

320 about 5% for both PM$_{10}$ and PM$_{2.5}$ on average over the domain.

For inorganic aerosols, ammonium concentrations using the stationary approach are larger (NME of 24%) than using the non-stationary approach. The concentration of nitrate in Case-5 is lower (NME of 13%). For organic aerosols, the differences are low (NME of 3%).

In Case-6, the Rosenbrock rather the ETR solver is used in the non-stationary approach. The simulated concentrations are

325 not sensitive to the solver used (time-averaged NME less than 1%).

For secondary compounds, such as NO$_2$, inorganic and organic aerosols, it is crucial to use the non-stationary approach, as it ensures numerical stability and strongly affects the concentrations.
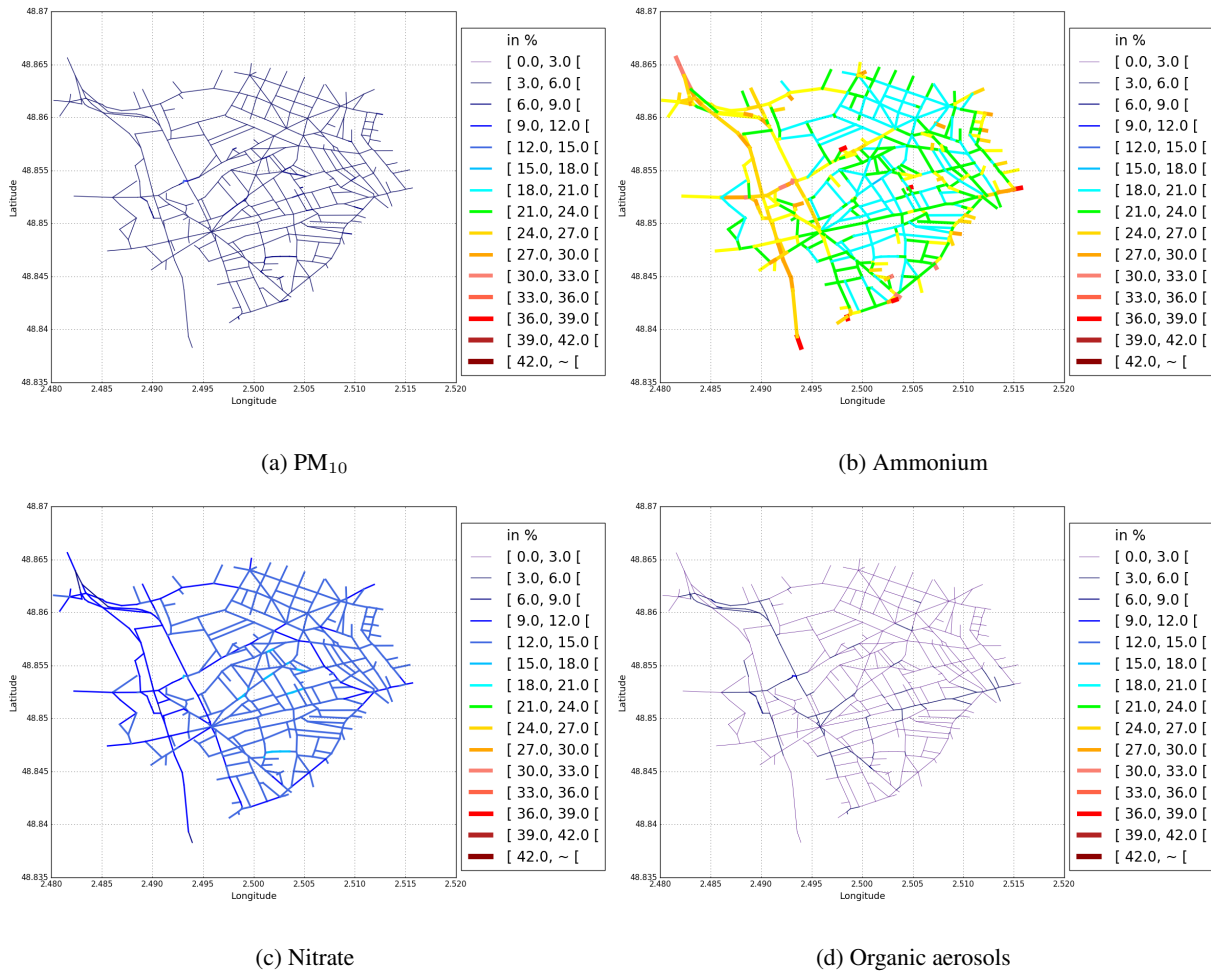
(a) PM$_{10}$

(b) Ammonium

(c) Nitrate

(d) Organic aerosols

Figure 11. Temporal NME (in %) between Case-1 and Case-5 for (a) PM$_{10}$, (b) Ammonium, (c) Nitrate and (d) Organic aerosols. The absolute differences in the concentrations between the simulations are presented in additional figures in Appendix C.

6   Parameters related to deposition and resuspension

In the Case-3 simulation, deposition is not taken into account. Very low differences are obtained between the Case-1 and Case-3 simulations.

Particle dry-deposition has a negligible impact on PM concentration over the simulation domain (the time-averaged NME is 1% for PM$_{2.5}$, see Table 4). The gas-phase deposition parameterisation also has a low impact on sulfur dioxide (SO$_2$) and ozone (O$_3$) concentrations (the NME is about 1% on average). It is however important to notice this conclusion does not take into account the potential role of the urban vegetation in the deposition process (Janhäll, 2015). Moreover the average building height in the considered district is rather low. The deposition process could have a more significant impact for more densely built urban area.

In the Case-4 simulation, a parameterisation for particle resuspension is used. The amount of resuspended mass in MUNICH is limited by the deposited mass (Lugon et al., 2021b). Because the deposited mass is not significant in Case-3, the resuspended mass in Case-4 is also low.

340   Dry-deposition on urban surfaces and resuspension have a low impact on concentrations in Paris. However, wet-deposition by rain may have a large impact during rainy days and should be considered (Roustan et al., 2010; Vivanco et al., 2018).

7   Sensitivity simulations

The street concentrations are strongly influenced by the building characteristics and by the traffic in the streets. To illustrate this influence, two sensitivity simulations are performed by arbitrarily modifying the building aspect ratio and by suppressing
345   the traffic in a street.

7.1   Influence of building aspect ratio

The building aspect ratio, which is the ratio of building height to street width (H/W), is an important characteristic of streets, because it influences the turbulent transfer of pollutants at roof level and the vertical wind profile in the streets (Kim et al., 2018).
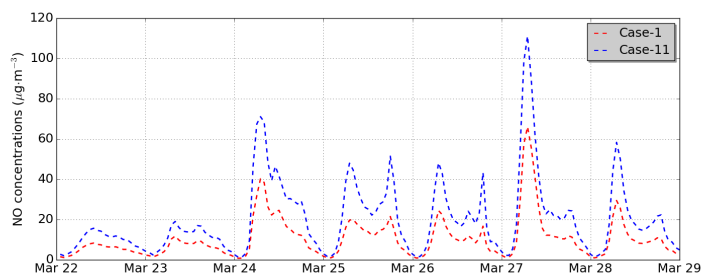
350   An additional sensitivity simulation (Case-11) is conducted to estimate the effect of the aspect ratio. The Case-1 reference simulation is repeated by artificially modifying the building height and the street width. The street width is reduced by a factor of $\sqrt{3}$ and the building height is increased by a factor of $\sqrt{3}$ for all street segments. Therefore the aspect ratio is increased by a factor of 3. Modifying both the building height and the street width is important so that the volume of the street segments is not changed. Figure 6d shows that the NME between the Case-1 and Case-11 simulations are high where the $PM_{2.5}$ concentrations
355   are high. Figure 12 shows the temporal variation of NO and NO_2 concentrations, which are averaged over the whole simulation domain (Case-1 and Case-11 simulations). The concentrations of NO and NO_2 in the Case-11 simulation are larger than those in the Case-1 simulation by the NME of 72% and 44%. The concentrations of $PM_{2.5}$ and PM_{10} also increase in the Case-11 simulation with NME of 16% and 17%, respectively. These larger concentrations are due to reduced turbulent transfer at roof level and reduced mean horizontal wind speed. Kim et al. (2018) estimated that the turbulent transfer decreases by 30% when
360   the aspect ratio increases by a factor of 2.

7.2   Effects of streets without cars

Many European cities have taken Low-Emission Zone (LEZ) measures to reduce street-level air pollution. The effects of this type of measure can be simulated by reducing emissions in specific streets. An additional sensitivity simulation (Case-12) is conducted to estimate the effects of emission reduction in a street. In the Case-12 simulation, the setup of the reference
365   simulation (Case-1) is used, but the emissions are set to zero in the Boulevard Alsace Lorraine (see Figure 4a). It means all vehicles are forbidden in this street. The background concentrations are the same in Case-12 as in the reference simulation,
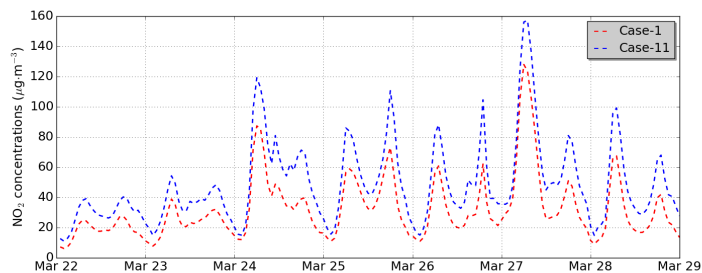
(a) NO$_2$

(b) NO

Figure 12. Comparison of the Case-1 hourly concentrations to the sensitivity simulation Case-11 modifying the building aspect ratio over the whole simulation domain: (a) NO$_2$ and (b) NO

meaning that the total emissions are the same in both simulations. However, we assume that traffic is redistributed in nearby streets of Boulevard Alsace Lorraine, but not directly adjacent.

Figure 13 shows the differences in NO$_2$ concentrations between Case-1 and Case-12 simulations. NO$_2$ concentration in Boulevard Alsace Lorraine with Case-12 simulation is lower than that with Case-1 simulation by 43% (Case-1: 44 μg m^{-3} vs Case-12: 25 μg m^{-3}). It shows that pollutant concentrations are not negligible even though they are not emitted in the street. It is due to the pollutant transfer from the overlying atmosphere and from the neighboring streets. However, they are strongly reduced. For PM$_{10}$ and PM$_{2.5}$, the reduction is lower than for NO$_2$ (18% for PM$_{10}$ and 16% for PM$_{2.5}$). This higher contribution of street emissions to concentrations for NO$_2$ than for PM is due to differences in the atmospheric processes leading to PM and NO$_2$ concentrations (longer atmospheric lifetimes and, therefore, larger contributions of the background leading to lower contributions of local PM emissions).

8 Conclusions

The street-network model MUNICH v2.0 is presented for multi-pollutant modelling in street canyons. A reference test case is set up in the East side of Greater Paris, where model to measurements are performed. NO$_2$, PM$_{2.5}$ and PM$_{10}$ are well modelled with MUNICH v2.0 compared to measurements.

(a) NO$_2$

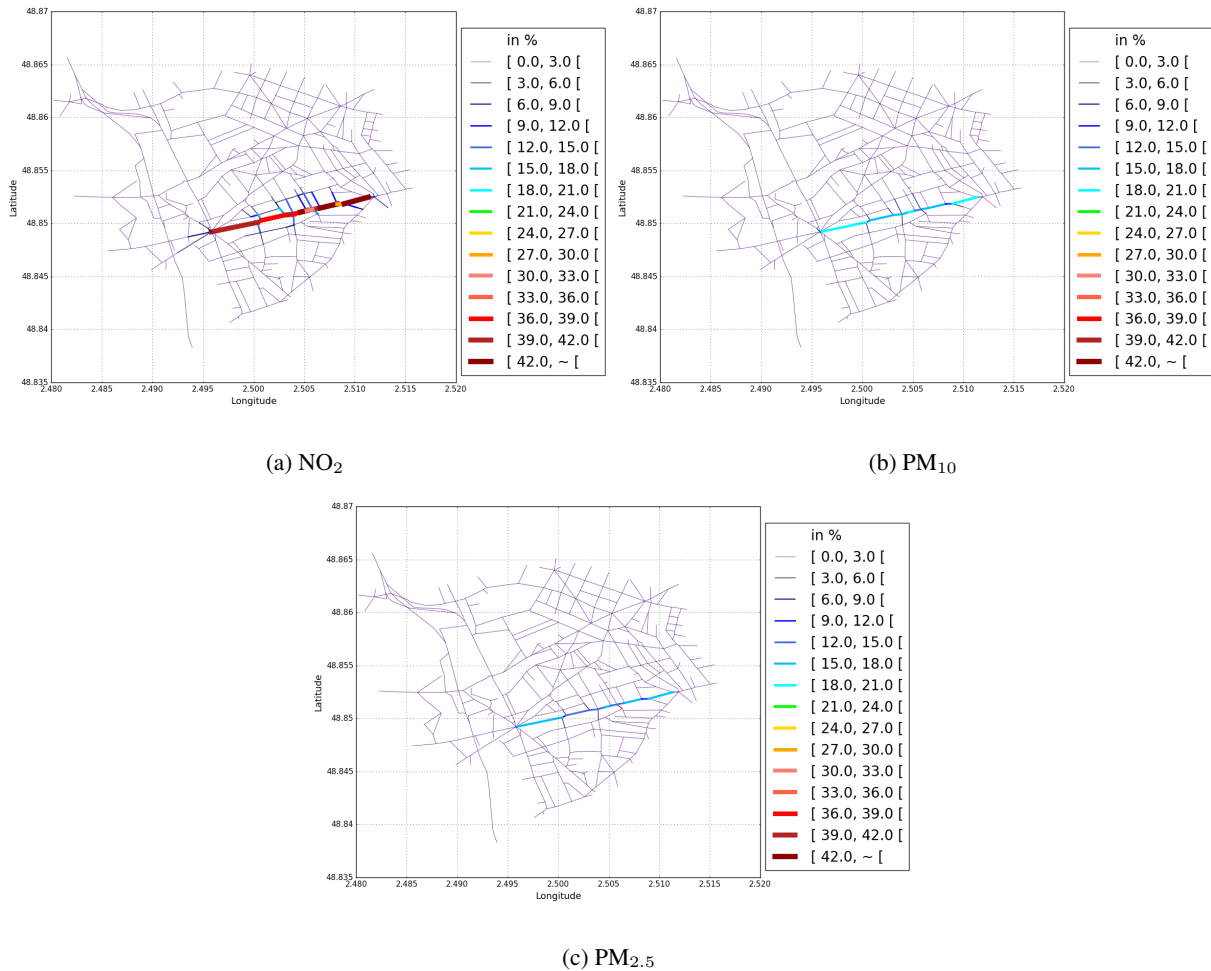(b) PM$_{10}$

(c) PM$_{2.5}$

Figure 13. Temporal NME (in %) between Case-1 and Case-12 for (a) NO$_2$ (b) PM$_{10}$ and (c) PM$_{2.5}$. The absolute differences in the concentrations between the simulations are presented in additional figures in Appendix C.

A new parameterisation to compute the wind velocity at the roof level leads to an increase in PM$_{2.5}$ (13%) and NO$_2$ (32%) concentrations at the air monitoring station near traffic. The turbulent vertical transfer increases with the parameterisation taking into account the building height. It is due to low building heights in the street network studied here. This high sensitivity to wind velocity at the roof level underlines the importance of meteorological down-scaling to accurately represent the transition from the regional to the street scale.

The SSH-aerosol model is implemented in MUNICH v2.0 for primary and secondary aerosol modelling in street canyons, taking into account gaseous chemistry leading to the formation of condensables, condensation/evaporation, nucleation and coagulation. The PM$_{10}$ and PM$_{2.5}$ concentrations increase by 11% and 13%, respectively, if SSH-aerosol is used. This increase is due to the formation of secondary inorganic and organic aerosols. The NO$_2$ concentration increases by 11% using SSH-

23

aerosol. A non-stationary approach is developed to model reactive pollutants. On average over the street-network considered, the non-stationary approach leads to a decrease in NO_2 concentration by 16% compared to the stationary approach.

In comparison to MUNICH v1.0, parameterisations of particle deposition and resuspension are also added in MUNICH v2.0. However their impact on pollutant concentrations in the street canyons is low for the considered domain.

MUNICH may be easily used with background concentrations from a regional air-quality model, in an one-way coupling approach. For the next step, the coupling between MUNICH v2.0 and regional air-quality model will be improved to consider two-way coupling. The coupled model will be an updated version of the Street-in-Grid model, which computes both the pollutant concentrations within the street network and the average concentrations for the overlying atmosphere grid at same time.

Code and data availability. MUNICH v2.0 is available at Kim et al. (2022) or git repository at https://github.com/cerea-lab/munich. The configuration files and input data of the simulations and also scripts for figures are provided at https://doi.org/10.5281/zenodo.6167477. A user manual is available at http://cerea.enpc.fr/munich/doc/munich-guide-v2.pdf. The software requirements and the license information are provided in the user manual.

Appendix A: Statistical indicators

Table A1. Definitions of the statistical indicators.

Indicators	Definitions
Fractional bias (FB)	$\dfrac{\overline{c} - \overline{o}}{(\overline{c} + \overline{o})/2}$
Mean fractional bias (MFB) and mean fractional error (MFE)	$\dfrac{1}{n} \sum_{i=1}^{n} \dfrac{c_i - o_i}{(c_i + o_i)/2} \quad \text{and} \quad \dfrac{1}{n} \sum_{i=1}^{n} \dfrac{\mid c_i - o_i \mid}{(c_i + o_i)/2}$
Normalized mean square error (NMSE)	$\dfrac{\sum_{i=1}^{n}(c_i - o_i)^2}{\sum_{i=1}^{n} c_i o_i}$
Correlation coefficient (R)	$\dfrac{\sum_{i=1}^{n}(c_i - \overline{c})(o_i - \overline{o})}{\sqrt{\sum_{i=1}^{n}(c_i - \overline{c})^2}\sqrt{\sum_{i=1}^{n}(o_i - \overline{o})^2}}$
Geometrical mean squared variance (VG)	$\exp\left(\dfrac{\sum_{i=1}^{n}\left((\ln(c_i) - \ln(o_i))^2\right)}{n}\right)$
Mean geometric bias (MG)	$\exp\left(\dfrac{\sum_{i=1}^{n}(\ln(c_i) - \ln(o_i))}{n}\right)$
Fraction of modeled values within a factor of two of observations (FAC2)	$0.5 \leq c_i/o_i \leq 2$
Normalized Absolute Difference (NAD)	$\dfrac{\frac{1}{n}\sum_{i=1}^{n} \mid c_i - o_i \mid}{\overline{c} + \overline{o}}$
Normalized Mean Error (NME)	$\dfrac{\frac{1}{n}\sum_{i=1}^{n} \mid c_i - o_i \mid}{\overline{o}}$

c_i: modeled values, o_i: observed values, n: number of data.

$$\overline{o} = \frac{1}{n}\sum_{i=1}^{n} o_i \quad \text{and} \quad \overline{c} = \frac{1}{n}\sum_{i=1}^{n} c_i$$

Appendix B: Modelling options in MUNICH

405 Several modelling options are available in MUNICH in order to handle the complexity and the computational time.

The options related with the modelling of the pollutant transport, deposition and resuspension are detailed here. Note that the options linked to the modelling of chemical transformations and aerosol dynamics are presented in the article describing the SSH-aerosol model (Sartelet et al., 2020).

First of all, it is useful to present the main equations solved in MUNICH before the presentation of the options.

410 The time variation of the mass M $\frac{dM}{dt}$ is computed using a transport-related term ($\frac{dM}{dt}|_{transp}$)and a chemistry-related term ($\frac{dM}{dt}|_{chem}$)

$$\frac{dM}{dt} = \frac{dM}{dt}|_{transp} + \frac{dM}{dt}|_{chem}.$$ (B1)

The transport-related term is computed as

$$\frac{dM}{dt}|_{transp} = Q_{inflow} + Q_{emis} - (Q_{outflow} + Q_{vert} + Q_{dep})$$ (B2)

415 where Q_{inflow} is the incoming flux to the street, Q_{emis} is the emission flux in the street, $Q_{outflow}$ is the outgoing flux from the street, Q_{vert} is the vertical exchange flux at the roof level, Q_{dep} is the deposition flux.

- With_stationary_hypothesis:
  whether the stationary hypothesis is assumed or not (available options: yes or no)

  If the stationary approach is used, the concentrations are computed in each street segment by assuming that $\frac{dM}{dt}|_{transp} =$
420 0. The non-stationary approach is recommended to model reactive species/pollutants. Note that the computation time increases by a factor 3 using the non-stationary approach for the reference test case (see section 2.3 and also 5.2).

- Numerical_method_parameterisation:
  numerical solver (available options: ETR or Rosenbrock) The solver used to solve Eq. B2 with the non-stationary approach may either be the Explicit Trapezoidale Rule (ETR) or Rosenbrock. If the ETR solver is used, Eq. B2 is discretized
425 as (Lugon et al., 2020):

$$C_s^{n+1} = C_s^n + \frac{\Delta t}{2} \left(F(C_s^n) + F(C_s^*) \right)$$ (B3)

$$C_s^* = C_s^n + \Delta t F(C_s^n)$$ (B4)

where s represents a chemical species (gas or particle), C_s^n is the concentration at time t^n, and $F(C_s^n)$ represents the
430 time derivative of C_s^n due to transport-related processes obtained by Eq. B2. The time step Δt is adjusted by

$$\Delta t^{n+1} = \Delta t^n \sqrt{\frac{\Delta_0}{\Delta_1}}$$ (B5)

where Δ_1 is the relative error and Δ_0 is the relative error precision which is set to 0.01. The relative error Δ_1 is computed as

$$\Delta_1 = \left\| \frac{C^{n+1} - C^*}{C^{n+1}} \right\|_2 \tag{B6}$$

where C is the vector of concentration for all chemical species. The Euclidean norm is used to compute the relative error so that the error for all species is averaged.

The Rosenbrock solver is implemented to improve numerical stability of the non-stationary approach:

$$C_s^{n+1} = C_s^n + \frac{3}{2}\Delta t k_1 + \frac{1}{2}\Delta t k_2 \tag{B7}$$

k_1 and k_2 are computed as

$$(1 - \gamma \Delta t J)k_1 = F(C_s^n) \tag{B8}$$

$$(1 - \gamma \Delta t J)k_2 = F(C_s^{n+1} + \gamma k_1) - 2k_1 \tag{B9}$$

where γ is $1 + \sqrt{2}/2$ and J is a Jacobian matrix of Eq B2.

- `Transfer_parameterisation`:

parameterisation to compute turbulent vertical mass transfer (available options: SIRANE or SCHULTE)

The vertical flux, Q_{vert} is formulated using the SIRANE option as follows:

$$Q_{\text{vert}} = \frac{\sigma_{\text{w}} W L}{\sqrt{2}\pi} \left(C_{\text{street}} - C_{\text{background}}\right) \tag{B10}$$

where $C_{\text{background}}$ is the mean concentration above the street segment, L is the street length, and σ_{w} is the standard deviation of the vertical wind velocity at roof level, which depends on atmospheric stability.

Using the SCHULTE option, the street aspect ratio (a_r, ratio of building height to street width) is taken into account:

$$Q_{\text{vert}} = 0.45 \sigma_{\text{w}} W L \left(\frac{1}{1 + a_r}\right) \left(C_{\text{street}} - C_{\text{background}}\right) \tag{B11}$$

where $a_r = H/W$

- `Building_height_wind_speed_parameterisation`:

parameterisation to compute wind speed at the roof level (available options: SIRANE or MACDONALD)

Using the SIRANE option (Soulhac et al., 2008), the wind speed at the roof level and at the center of the street (u_M) is computed as

$$u_M = u_* \sqrt{\frac{\pi}{\sqrt{2}\kappa^2 C} \left(Y_0(C) - \frac{J_0(C)Y_1(C)}{J_1(C)}\right)} \tag{B12}$$

where u_* is the friction velocity, J_0, J_1 and Y_1 are Bessel functions. κ is the von Kármán constant. To compute the mean wind speed at the roof level over the street width (u_H), the horizontal wind speed variation of Soulhac et al. (2008) is considered. As discussed in Section 2.2, using the MACDONALD option, the wind speed at the roof level (u_H) is computed as

$$u_H = \frac{u_*}{\kappa} \ln\left(\frac{H - d_c}{z_{0_c}}\right) = u_{ref} \times \frac{\ln\left(\frac{H - d_c}{z_{0_c}}\right)}{\ln\left(\frac{z_{ref} - d_c}{z_{0_c}}\right)}. \tag{B13}$$

- Mean_wind_speed_parameterisation:

parameterisation to compute mean wind speed within the street canyon (available options: Exponential or SIRANE)

Using the Exponential option (Lemonsu et al., 2004), the wind speed within the street canyon is computed as

$$u_{street} = u_H |\cos(\varphi)| \frac{2}{a_r}\left(1 - \exp\left(\frac{a_r}{2}\left(\frac{z_0}{H} - 1\right)\right)\right) \tag{B14}$$

where u_H represents the wind speed at the roof level and is computed by the option detailed above (see section 2.2), φ is the angle between the street orientation and the wind direction, z_0 is the aerodynamic roughness of canyon surfaces.

Using the SIRANE option (Eq (1) in Soulhac et al. (2011)), the wind speed within the street canyon is computed as

$$u_{street} = u_M |\cos(\varphi)| \frac{\delta_i^2}{HW}\left(\frac{2\sqrt{2}}{C}(1 - \beta)\left(1 - \frac{C^2}{3} + \frac{C^4}{45}\right) + \beta \frac{2\alpha - 3}{\alpha} + \left(\frac{W}{\delta_i} - 2\right)\frac{\alpha - 1}{\alpha}\right) \tag{B15}$$

where $\delta_i = min(H, W/2)$, $\alpha = ln\frac{\delta_i}{z_0}$, $\beta = exp\left(\frac{C}{\sqrt{2}}\left(1 - \frac{H}{\delta_i}\right)\right)$, C is a solution of $\frac{z_0}{\delta_i} = \frac{2}{C}exp\left(\frac{\pi}{2}\frac{Y_1(C)}{J_1(C)} - 0.577\right)$

- With_horizontal_fluctuation:

whether turbulent mixing at intersection via the horizontal fluctuation of the wind direction is taken into account or not (available options: yes or no)

The horizontal fluctuation of the wind direction represents the turbulent mixing of the air across the intersection (Soulhac et al., 2008). The fluctuation is computed by the following steps:

1. When the fluctuation is not taken into account, the air flux from street i to street j, $P_{i,j}$ for the wind direction φ is computed using the outgoing flux and the incoming flux at Eq. B2.

2. Compute N times, the air flux $P_{i,j}(\varphi + \sigma)$ for the wind direction $\varphi + \sigma$ where σ is the fluctuation of the wind direction ranging from -20° to 20°. N is the number of σ values. N is 10 when σ is 20°

3. Compute the sum of the air flux.

$$P_{i,j} = \sum f(\sigma) P_{i,j}(\varphi + \sigma) \tag{B16}$$

where $f(\sigma)$ is a Gaussian distribution of the wind direction ranging from 0 to 1.

- Deposition_wind_profile:

wind profile option for dry deposition (available options: MASSON or MACDONALD)

The friction velocity is used to compute the deposition as follows:

$$u_* = \kappa \, exp\left(p(\frac{z}{h} - 1)/log(z/z_0)\right) \tag{B17}$$

where p is the parameter for the wind profile.

The parameter p may be computed using the MASSON option

$$p = 0.5 \, \frac{H}{W}, \tag{B18}$$

or using the MACDONALD option

$$p = 9.6 \, \lambda_f \tag{B19}$$

where $\lambda_f = \frac{H}{W + \frac{\lambda_p W}{1 - \lambda_p}}$ and λ_p is the building density.

- Particles_dry_velocity_option:

parameterisation for aerosol deposition (available options: Zhang, Giardina, Venkatram or Muyshondt)

Using the Zhang option (Zhang et al., 2001), the deposition velocity is computed as

$$v_d = v_s + \frac{1}{R_{street}} \tag{B20}$$

where R_{street} is the total resistance of the aerodynamic resistance of the street and the surface resistance and v_s is the sedimentation velocity.

Using the Giardina option (Giardina and Buffa, 2018), the deposition velocity is computed as

$$v_d = v_s/(1 - exp^{v_s(Ra_{street} + \frac{1}{R_{eq}})}) \tag{B21}$$

where Ra_{street} is the sum of the aerodynamic resistance of the street and R_{eq} represents the resistance by the Brownian diffusion.

Using the Venkatram option (Venkatram and Pleim, 1999), the deposition velocity is computed as

$$v_d = v_s/(1 - exp^{v_s R_{street}}) \tag{B22}$$

Using the Muyshondt option (Muyshondt et al., 1996), the deposition velocity is computed as

$$v_d = v_s + v_{Re} \tag{B23}$$

where v_{Re} represents the influence of the Reynolds number on the deposition velocity.

29

Dry-deposition on urban surfaces and resuspension have a low impact on concentrations in Paris. However, wet-deposition by rain may have a large impact during rainy days and should be considered (Roustan et al., 2010; Vivanco et al., 2018). measured and simulated particle deposition over the street surface.

- `With_resuspension:`
  whether the resuspension is taken into account or not (available options: yes or no)

  Particle resuspension is computed based on a resuspension factor f_{res}

$$f_{res} = \sum_{v=1}^{2} N_v \left(\frac{u_v}{u_{ref}(r)} \right) f_{0,v} \tag{B24}$$

where v indicates the vehicle type, N_v is the vehicle flow (vehicles per hour), u_v is the vehicle speed ($km\ h^{-1}$), $u_{ref}(r)$ is the reference vehicle speed for the resuspension process ($km\ h^{-1}$), and $f_{0,v}$ the reference mass fraction of the resuspension process (per vehicle). It is detailed in Lugon et al. (2021b).

- `With_drainage_aerosol:`
  whether drainage is taken into account or not (available options: yes or no)

$$f_{wash} = \frac{1}{\delta t} \left(1 - exp\left(-h_{drain,eff} \frac{g_{road} - g_{road,min}}{g_{road,min}} \right) \right) \tag{B25}$$

where δt is the time, $h_{drain,eff}$ is the drainage efficiency parameter, g_{road} is the amount of water present on the street surface (mm), and $g_{road,min}$ is the minimum water content for the drainage process (mm).

When this option is used, the wash-off factors are computed and associated with the precipitation. It is detailed in Lugon et al. (2021b).

- `With_chemistry:`
  whether chemistry is taken into account or not (available options: yes or no)

  SSH-aerosol model is used when this option is set to yes. The options for the chemistry model are defined in the namelist of SSH-aerosol, namelist.ssh.
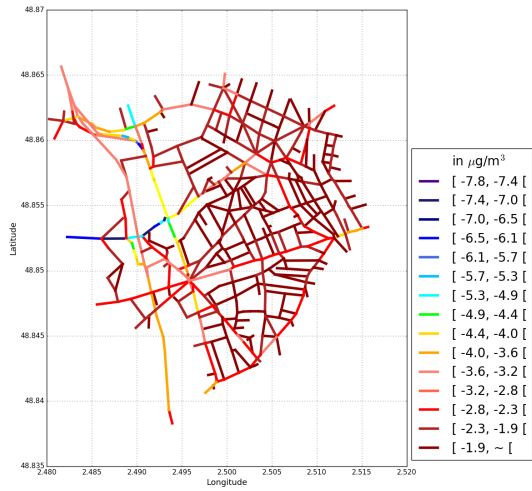
Appendix C: Absolute differences in the concentrations
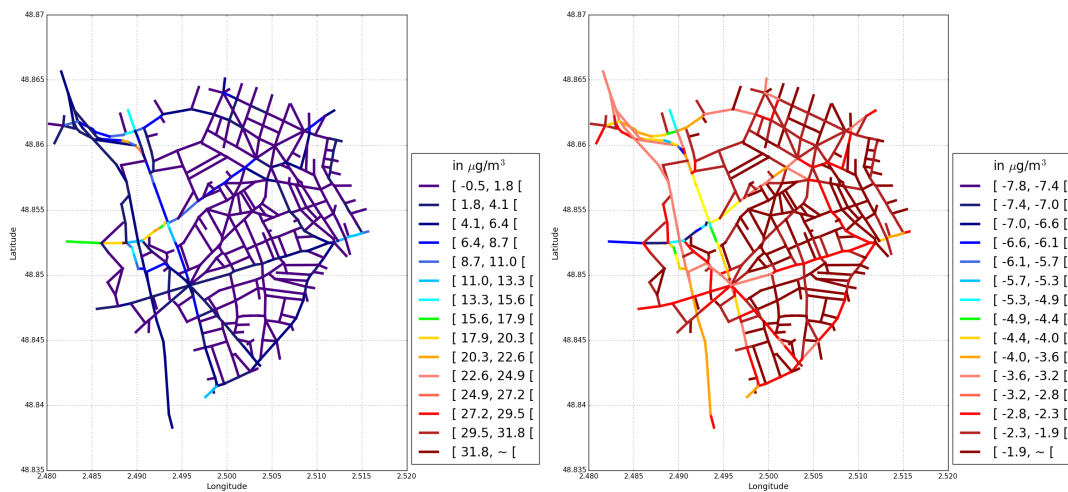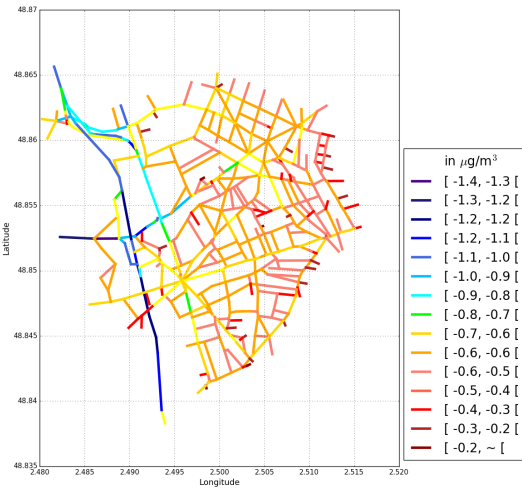

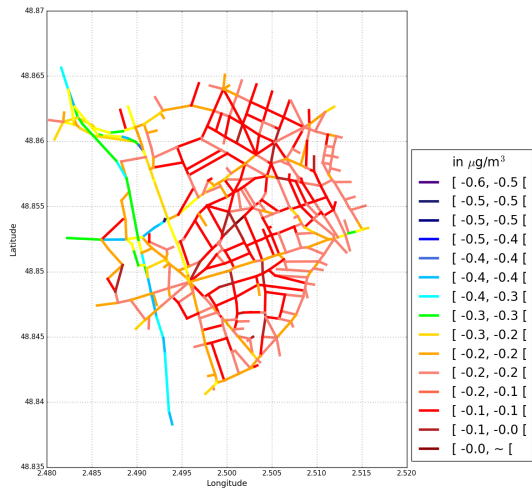(a) Case-10 - Case-1

(b) Case-2 - Case-1
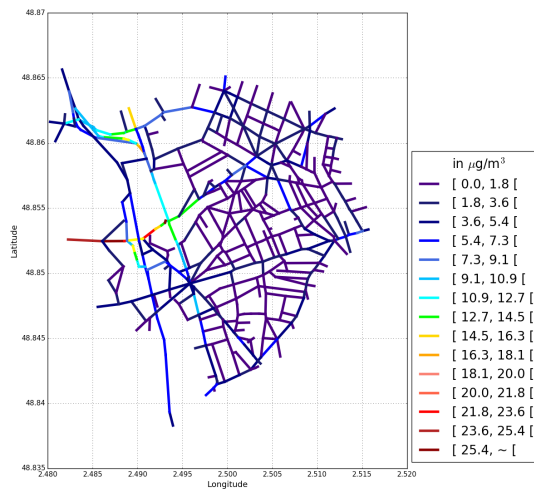
(c) Case-11 - Case-1

Figure C1. Differences in PM$_{2.5}$ time-averaged concentrations (in $\mu g\,m^{-3}$) between the reference test case (Case-1) and a sensitivity test case.
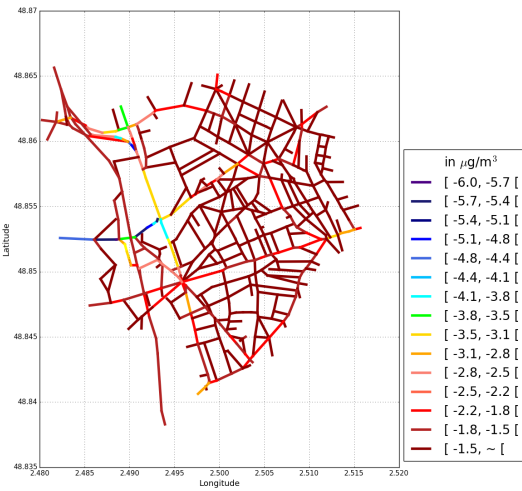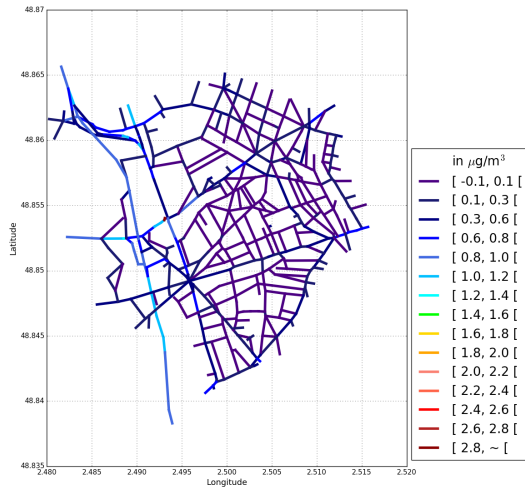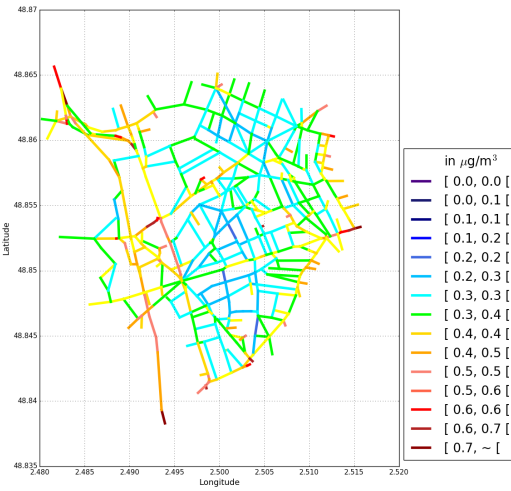
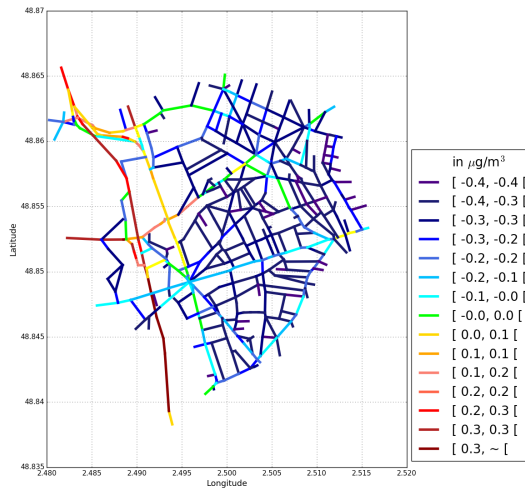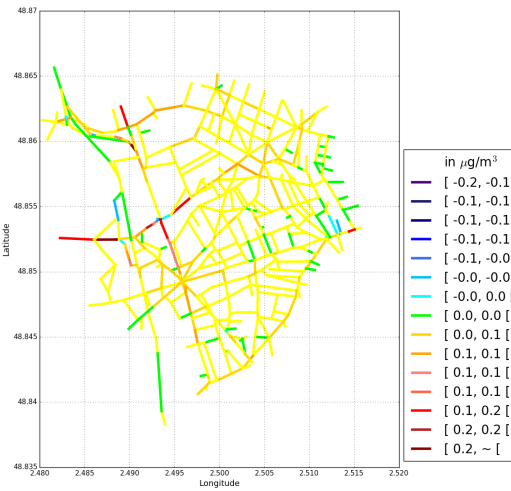(a) PM$_{10}$

(b) Ammonium

(c) Nitrate

(d) Organic aerosols

Figure C2. Differences in time-averaged concentrations (in $\mu g\,m^{-3}$) between Case-2 and Case-1 (Case-2 - Case-1) for (a) PM$_{10}$ (b) Ammonium (c) Nitrate and (d) Organic aerosols.
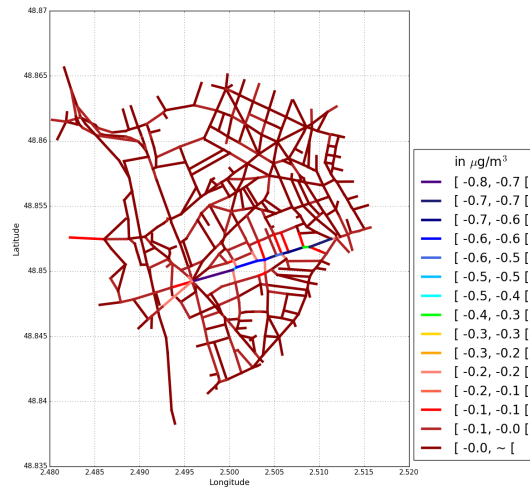
(a) PM$_{10}$

(b) Ammonium

(c) Nitrate

(d) Organic aerosols

Figure C3. Differences in time-averaged concentrations (in $\mu g \, m^{-3}$) between Case-5 and Case-1 (Case-5 - Case-1) for (a) PM$_{10}$ (b) Ammonium (c) Nitrate and (d) Organic aerosols.
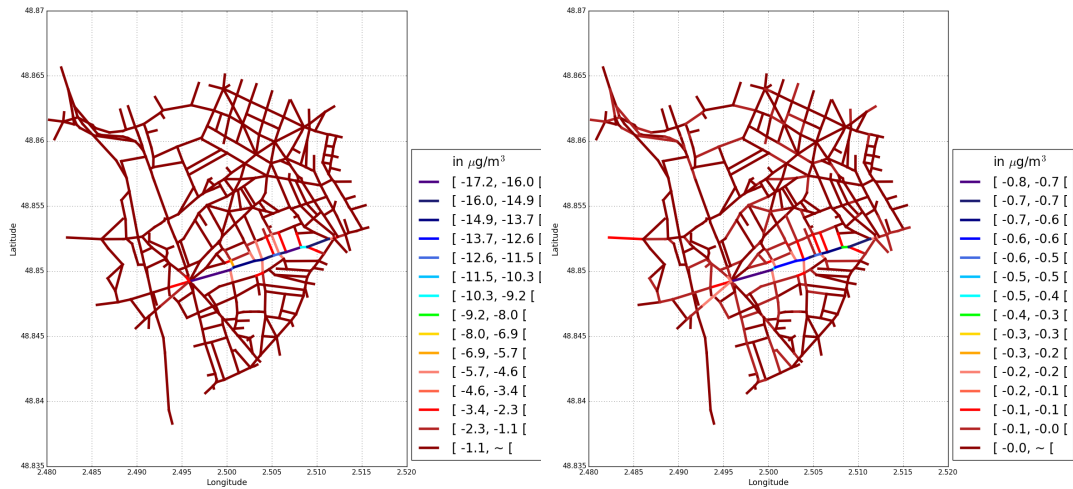
(a) NO$_2$

(b) PM$_{10}$

(c) PM$_{2.5}$

Figure C4. Differences in time-averaged concentrations (in μg m^{-3}) between Case-12 and Case-1 (Case-12 - Case-1) for (a) NO$_2$ (b) PM$_{10}$ (c) PM$_{2.5}$.

535

References

Airparif: Source apportionment of airbone particles in the Île-de-France region - Final report (INIS-FR–20-1041), available at https://inis.iaea.org/search/search.aspx?orig_q=RN:51070022, last access 15 February 2022, 2011.

André, M., Sartelet, K., Moukhtar, S., André, J.-M., and Redaelli, M.: Diesel, petrol or electric vehicles: What choices to improve urban air quality in the Ile-de-France region? A simulation platform and case study, Atmos. Environ., 241, 117 752, https://doi.org/10.1016/j.atmosenv.2020.117752, 2020.

André, M. et al.: Particules de l'air extérieur - Impact sur la pollution atmosphérique des technologies et de la composition du parc de véhicules automobiles circulant en France, 2014-SA-0156, ANSES, available at https://www.anses.fr/fr/system/files/AIR2014SA0156Ra-Emission.pdf, last access 7 December 2021, 2019.

Benson, P. E.: A review of the development and application of the CALINE3 and 4 models, Atmos. Environ., 26, 379–390, https://doi.org/10.1016/0957-1272(92)90013-I, 1992.

Berkowicz, R.: OSPM - a parameterised street pollution model, Environ. Monit. Assess., 65, 323 – 331, https://doi.org/10.1023/A:1006448321977, 2000.

Briant, R., Seigneur, C., Gadrat, M., and Bugajny, C.: Evaluation of roadway Gaussian plume models with large-scale measurement campaigns, Geosci. Model Dev., 6, 445–456, https://doi.org/10.5194/gmd-6-445-2013, 2013.

Cherin, N., Roustan, Y., Musson-Genon, L., and Seigneur, C.: Modelling atmospheric dry deposition in urban areas using an urban canopy approach, Geosci. Model Dev., 8, 893–910, https://doi.org/10.5194/gmd-8-893-2015, 2015.

Chrit, M., Sartelet, K., Sciare, J., Pey, J., Marchand, N., Couvidat, F., Sellegri, K., and Beekmann, M.: Modelling organic aerosol concentrations and properties during ChArMEx summer campaigns of 2012 and 2013 in the western Mediterranean region, Atmos. Chem. Phys., 17, 12 509–12 531, https://doi.org/10.5194/acp-17-12509-2017, 2017.

Cyrys, J., Eeftens, M., Heinrich, J., Ampe, C., Armengaud, A., Beelen, R., Bellander, T., Beregszaszi, T., Birk, M., Cesaroni, G., Cirach, M., de Hoogh, K., De Nazelle, A., de Vocht, F., Declercq, C., Dědelė, A., Dimakopoulou, K., Eriksen, K., Galassi, C., Grąulevičienė, R., Grivas, G., Gruzieva, O., Gustafsson, A. H., Hoffmann, B., Iakovides, M., Ineichen, A., Krämer, U., Lanki, T., Lozano, P., Madsen, C., Meliefste, K., Modig, L., Mölter, A., Mosler, G., Nieuwenhuijsen, M., Nonnemacher, M., Oldenwening, M., Peters, A., Pontet, S., Probst-Hensch, N., Quass, U., Raaschou-Nielsen, O., Ranzi, A., Sugiri, D., Stephanou, E. G., Taimisto, P., Tsai, M.-Y., Éva Vaskövi, Villani, S., Wang, M., Brunekreef, B., and Hoek, G.: Variation of NO_2 and NOx concentrations between and within 36 European study areas: Results from the ESCAPE study, Atmos. Environ., 62, 374–390, https://doi.org/10.1016/j.atmosenv.2012.07.080, 2012.

EMEP/EEA: EMEP/EEA air pollutant emission inventory guidebook 2019, EEA Report No 13/2019, European Environment Agency, available at https://www.eea.europa.eu/publications/emep-eea-guidebook-2019, last access 7 December 2021, 2019.

Giardina, M. and Buffa, P.: A new approach for modeling dry deposition velocity of particles, Atmos. Environ., 180, 11–22, https://doi.org/10.1016/j.atmosenv.2018.02.038, 2018.

Hanna, S. and Chang, J.: Acceptance criteria for urban dispersion model evaluation, Meteorol. Atmos. Phys., 116, 133–146, https://doi.org/10.1007/s00703-011-0177-1, 2012.

Herring, S. and Huq, P.: A review of methodology for evaluating the performance of atmospheric transport and dispersion models and suggested protocol for providing more informative results, Fluids, 3, https://doi.org/10.3390/fluids3010020, 2018.

Janhäll, S.: Review on urban vegetation and particle air pollution - Deposition and dispersion, Atmospheric Environment, 105, 130–137, https://doi.org/10.1016/j.atmosenv.2015.01.052, 2015.

575   Jeanjean, A., Hinchliffe, G., McMullan, W., Monks, P., and Leigh, R.: A CFD study on the effectiveness of trees to disperse road traffic emissions at a city scale, Atmos. Environ., 120, 1–14, https://doi.org/10.1016/j.atmosenv.2015.08.003, 2015.

Kim, Y., Couvidat, F., Sartelet, K., and Seigneur, C.: Comparison of different gas-phase mechanisms and aerosol modules for simulating particulate matter formation, J. Air Waste Manage. Assoc., 61, 1–9, https://doi.org/10.1080/10473289.2011.603999, 2011.

Kim, Y., Wu, Y., Seigneur, C., and Roustan, Y.: Multi-scale modeling of urban air pollution: development and application of a Street-in-Grid

580   model (v1.0) by coupling MUNICH (v1.0) and Polair3D (v1.8.1), Geosci. Model Dev., 11, 611–629, https://doi.org/10.5194/gmd-11-611-2018, 2018.

Kim, Y., Sartelet, K., Lugon, L., Roustan, Y., Sarica, T., Maison, A., Valari, M., Zhang, Y., and André, M.: The Model of Urban Network of Intersecting Canyons and Highways (MUNICH) v2.0, Zenodo, https://doi.org/10.5281/zenodo.6167477, 2022.

Krzyzanowski, M., Apte, J., Bonjour, S., Brauer, M., Cohen, A., and Prüss-Ustun, A.: Air pollution in the mega-cities, Curr. Environ. Health

585   Rep., 1, 185–191, https://doi.org/10.1007/s40572-014-0019-7, 2014.

Kusaka, H., Kondo, H., Kikegawa, Y., and Kimura, F.: A simple single-layer urban canopy model for atmospheric models: comparison with multi-layer and slab models, Bound.-Lay. Meteorol., 101, 329–358, https://doi.org/10.1023/A:1019207923078, 2001.

Leclercq, L., Laval, J. A., and Chevallier, E.: The Lagrangian coordinates and what it means for first order traffic flow models, Proceedings of the 17th international symposium on transportation and traffic theory, pp. 735–753, ed.: Allsop, R.E., Bell, M.G.H., Heydecker, B.G.,

590   Elsevier, London, 2007.

Lemonsu, A., Grimmond, C. S. B., and Masson, V.: Modeling the surface energy balance of the core of an old Mediterranean city: Marseille., J. Appl. Meteorol., 43, 312–327, https://doi.org/10.1175/1520-0450(2004)043<0312:MTSEBO>2.0.CO;2, 2004.

Lugon, L., Sartelet, K., Kim, Y., Vigneron, J., and Chrétien, O.: Nonstationary modeling of NO_2, NO and NO_x in Paris using the Street-in-Grid model: coupling local and regional scales with a two-way dynamic approach, Atmos. Chem. Phys., 20, 7717–7740,

595   https://doi.org/10.5194/acp-20-7717-2020, 2020.

Lugon, L., Sartelet, K., Kim, Y., Vigneron, J., and Chrétien, O.: Simulation of primary and secondary particles in the streets of Paris using MUNICH, Faraday Discuss., 226, 432–456, https://doi.org/10.1039/D0FD00092B, 2021a.

Lugon, L., Vigneron, J., Debert, C., Chrétien, O., and Sartelet, K.: Black carbon modeling in urban areas: investigating the influence of resuspension and non-exhaust emissions in streets using the Street-in-Grid model for inert particles (SinG-inert), Geosci. Model Dev., 14,

600   7001–7019, https://doi.org/10.5194/gmd-14-7001-2021, 2021b.

Macdonald, R., Griffiths, R., and Hall, D.: An improved method for the estimation of surface roughness of obstacle arrays, Atmos. Environ., 32, 1857–1864, https://doi.org/10.1016/S1352-2310(97)00403-2, 1998.

Maison, A., Flageul, C., Carissimo, B., Tuzet, A., and Sartelet, K.: Parametrization of Horizontal and Vertical Transfers for the Street-Network Model MUNICH Using the CFD Model Code_Saturne, Atmosphere, 13, 527, https://doi.org/10.3390/atmos13040527, 2022.

605   McHugh, C., Carruthers, D., and Edmunds, H.: ADMS–Urban: an air quality management system for traffic, domestic and industrial pollution, Int. J. Environ. Pollut., 8, 666–674, https://doi.org/10.1504/IJEP.1997.028218, 1997.

Milliez, M. and Carissimo, B.: Numerical simulations of pollutant dispersion in an idealized urban area, for different meteorological conditions, Boundary-Layer Meteorol, 122, 321–342, https://doi.org/10.1007/s10546-006-9110-4, 2007.

Muyshondt, A., Anand, N. K., and McFarland, A. R.: Turbulent deposition of aerosol particles in large transport tubes, Aerosol Sci. Technol.,

610   24, 107–116, https://doi.org/10.1080/02786829608965356, 1996.

Namdeo, A. and Colls, J.: Development and evaluation of SBLINE, a suite of models for the prediction of pollution concentrations from vehicles in urban areas, Sci. Total Environ., 189-190, 311–320, https://doi.org/10.1016/0048-9697(96)05224-2, 1996.

Putaud, J.-P., Van Dingenen, R., Alastuey, A., Bauer, H., Birmili, W., Cyrys, J., Flentje, H., Fuzzi, S., Gehrig, R., Hansson, H., Harrison, R., Herrmann, H., Hitzenberger, R., Hüglin, C., Jones, A., Kasper-Giebl, A., Kiss, G., Kousa, A., Kuhlbusch, T., Löschau, G., Maenhaut, W., Molnar, A., Moreno, T., Pekkanen, J., Perrino, C., Pitz, M., Puxbaum, H., Querol, X., Rodriguez, S., Salma, I., Schwarz, J., Smolik, J., Schneider, J., Spindler, G., ten Brink, H., Tursic, J., Viana, M., Wiedensohler, A., and Raes, F.: A European aerosol phenomenology - 3: Physical and chemical characteristics of particulate matter from 60 rural, urban, and kerbside sites across Europe, Atmos. Environ., 44, 1308–1320, https://doi.org/10.1016/j.atmosenv.2009.12.011, 2010.

Ritchie, H. and Roser, M.: Urbanization, Our world in data, available at https://ourworldindata.org/urbanization, last access 8 December 2021, 2018.

Roustan, Y., Sartelet, K., Tombette, M., Debry, É., and Sportisse, B.: Simulation of aerosols and gas-phase species over Europe with the Polyphemus system. Part II: Model sensitivity analysis for 2001, Atmos. Environ., 44, 4219–4229, https://doi.org/10.1016/j.atmosenv.2010.07.005, 2010.

Salizzoni, P., Soulhac, L., and Mejean, P.: Street canyon ventilation and atmospheric turbulence, Atmos. Environ., 43, 5056 – 5067, https://doi.org/10.1016/j.atmosenv.2009.06.045, 2009.

Santiago, J.-L., Rivas, E., Sanchez, B., Buccolieri, R., and Martin, F.: The impact of planting trees on NOx concentrations: the case of the Plaza de la Cruz neighborhood in Pamplona (Spain), Atmosphere, 8, https://doi.org/10.3390/atmos8070131, 2017.

Sarica, T.: Pollemission: computational tool for air pollutant emission factors from traffic (2.0), Zenodo, https://doi.org/10.5281/zenodo.5721253, 2021.

Sartelet, K., Zhu, S., Moukhtar, S., André, M., André, J.-M., Gros, V., Favez, O., Brasseur, A., and Redaelli, M.: Emission of intermediate, semi and low volatile organic compounds from traffic and their impact on secondary organic aerosol concentrations over Greater Paris, Atmos. Environ., 180, 126–137, https://doi.org/10.1016/j.atmosenv.2018.02.031, 2018.

Sartelet, K., Couvidat, F., Wang, Z., Flageul, C., and Kim, Y.: SSH-Aerosol v1.1: a modular box model to simulate the evolution of primary and secondary aerosols, Atmosphere, 11, https://doi.org/10.3390/atmos11050525, 2020.

Sartelet, K. N., Debry, É., Fahey, K., Roustan, Y., Tombette, M., and Sportisse, B.: Simulation of aerosols and gas-phase species over Europe with the Polyphemus system: Part I–Model-to-data comparison for 2001, Atmos. Environ., 41, 6116–6131, https://doi.org/10.1016/j.atmosenv.2007.04.024, 2007.

Schulte, N., Tan, S., and Venkatram, A.: The ratio of effective building height to street width governs dispersion of local vehicle emissions, Atmos. Environ., 112, 54 – 63, https://doi.org/10.1016/j.atmosenv.2015.03.061, 2015.

Skamarock, W. C., Klemp, J. B., Dudhia, J., Gill, D. O., Barker, D. M., Duda, M. G., Huang, X.-Y., Wang, W., and Powers, J. G.: A description of the Advanced Research WRF version 3, (No. NCAR/TN-475+STR). University Corporation for Atmospheric Research available at: http://dx.doi.org/10.5065/D68S4MVH, 2008.

Soulhac, L., Perkins, R. J., and Salizzoni, P.: Flow in a street canyon for any external wind direction, Bound.-Lay. Meteorol., 126, 365–388, https://doi.org/10.1007/s10546-007-9238-x, 2008.

Soulhac, L., Garbero, V., Salizzoni, P., Mejean, P., and Perkins, R.: Flow and dispersion in street intersections, Atmos. Environ., 43, 2981 – 2996, https://doi.org/10.1016/j.atmosenv.2009.02.061, 2009.

Soulhac, L., Salizzoni, P., Cierco, F.-X., and Perkins, R.: The model SIRANE for atmospheric urban pollutant dispersion; part I, presentation of the model, Atmos. Environ., 45, 7379 – 7395, https://doi.org/10.1016/j.atmosenv.2011.07.008, 2011.

Thouron, L., Kim, Y., Seigneur, C., and Bruge, B.: Intercomparison of two modeling approaches for traffic air pollution in street canyons, Urban Clim., 27, 163 – 178, https://doi.org/10.1016/j.uclim.2018.11.006, 2019.

Vardoulakis, S., Fisher, B. E., Pericleous, K., and Gonzalez-Flesca, N.: Modelling air quality in street canyons: a review, Atmos. Environ., 37, 155–182, https://doi.org/10.1016/S1352-2310(02)00857-9, 2003.

Venkatram, A. and Pleim, J.: The electrical analogy does not apply to modeling dry deposition of particles, Atmos. Environ., 33, 3075–3076, https://doi.org/10.1016/S1352-2310(99)00094-1, 1999.

655   Vivanco, M. G., Theobald, M. R., García-Gómez, H., Garrido, J. L., Prank, M., Aas, W., Adani, M., Alyuz, U., Andersson, C., Bellasio, R., Bessagnet, B., Bianconi, R., Bieser, J., Brandt, J., Briganti, G., Cappelletti, A., Curci, G., Christensen, J. H., Colette, A., Couvidat, F., Cuvelier, C., D'Isidoro, M., Flemming, J., Fraser, A., Geels, C., Hansen, K. M., Hogrefe, C., Im, U., Jorba, O., Kitwiroon, N., Manders, A., Mircea, M., Otero, N., Pay, M.-T., Pozzoli, L., Solazzo, E., Tsyro, S., Unal, A., Wind, P., and Galmarini, S.: Modeled deposition of nitrogen and sulfur in Europe estimated by 14 air quality model systems: evaluation, effects of changes in emissions and implications for
660   habitat protection, Atmos. Chem. Phys., 18, 10 199–10 218, https://doi.org/10.5194/acp-18-10199-2018, 2018.

Wolf, T., Pettersson, L. H., and Esau, I.: A very high-resolution assessment and modelling of urban air quality, Atmos. Chem. Phys., 20, 625–647, https://doi.org/10.5194/acp-20-625-2020, 2020.

Wu, L., Hang, J., Wang, X., Shao, M., and Gong, C.: APFoam 1.0: integrated computational fluid dynamics simulation of O_3–NO_x–volatile organic compound chemistry and pollutant dispersion in a typical street canyon, Geosci. Model Dev., 14, 4655–4681,
665   https://doi.org/10.5194/gmd-14-4655-2021, 2021.

Yarwood, G., Rao, S., Yocke, M., and Whitten, G.: Updates to the carbon bond chemical mechanism: CB05. Rep. RT-0400675, available at https://camx-wp.azurewebsites.net/Files/CB05_Final_Report_120805.pdf, last access 8 December 2021, 2005.

Zhang, L., Gong, S., Padro, J., and Barrie, L.: A size-segregated particle dry deposition scheme for an atmospheric aerosol module, Atmos. Environ., 35, 549–560, https://doi.org/10.1016/S1352-2310(00)00326-5, 2001.

670   Zhang, Y., Ye, X., Wang, S., He, X., Dong, L., Zhang, N., Wang, H., Wang, Z., Ma, Y., Wang, L., Chi, X., Ding, A., Yao, M., Li, Y., Li, Q., Zhang, L., and Xiao, Y.: Large-eddy simulation of traffic-related air pollution at a very high resolution in a mega-city: evaluation against mobile sensors and insights for influencing factors, Atmos. Chem. Phys., 21, 2917–2929, https://doi.org/10.5194/acp-21-2917-2021, 2021.